Renewable and Sustainable Energy Reviews 143 (2021) 110878

Contents lists available at ScienceDirect

Renewable and Sustainable Energy Reviews

journal homepage: http://www.elsevier.com/locate/rser

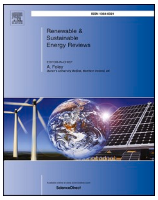

Sustainable MXenes-based membranes for highly energy-efficient separations

Mashallah Rezakazemi[a,*,1], Ahmad Arabi Shamsabadi[b,1], Haiqing Lin[c], Patricia Luis[d], Seeram Ramakrishna[e], Tejraj M. Aminabhavi[f]

[a] Faculty of Chemical and Materials Engineering, Shahrood University of Technology, Shahrood, Iran
[b] Department of Chemical and Biological Engineering, Drexel University, Philadelphia, PA, 19104, USA
[c] Department of Chemical and Biological Engineering, University of Buffalo, Buffalo, NY, 14260, USA
[d] Materials & Process Engineering (iMMC-IMAP), UCLouvain, Place Sainte Barbe 2, 1348, Louvain-la-Neuve, Belgium
[e] Nanoscience and Nanotechnology Initiative, National University of Singapore, Singapore, 1157, Singapore
[f] Department of Chemistry, Karnatak University, Dharwad, 580003, India

ARTICLE INFO

Keywords:
MXene
2D nanomaterials
Membrane
Gas and liquid separations
Desalination

ABSTRACT

The ease of producing two-dimensional (2D) structure, tunable surface chemistry, and interlayer spacing of MXenes have created innumerable opportunities for researchers to prepare such novel emergent materials as energy-efficient membranes in a variety of engineering separations. In this review, various methods used for the synthesis of MXenes, their functionalization and membrane fabrication are discussed with potential examples. The engineering as well as the design of atomically thin 2D MXene membranes developed over the past decade have played a major role in high-throughput separation areas. The fascinating features of MXenes in terms of ultrathin structure, tunable interlayer distance, versatile chemistry, and appealing physiochemical properties render themselves to be developed as membranes for use in numerous applications, such as in gas separation, liquid separation, and desalination. These applications are critically discussed in this review in terms of their current challenges and future directions as effective emergent membranes in industrial separation processes.

1. Introduction

In nanomaterials science, a young group of two-dimensional (2D) materials, called transition metal carbides and nitrides (MXenes), have attracted much interests over the past years [1–3]. In recent years, these MXenes have a great promise for a wide range of separation applications due to their superior chemical, mechanical, thermal, and separation properties [4,5]. The membranes, MXenes with 3, 5, or 7 atomic layer-thick compounds, are now regarded to be one of the atomically ultra-thin molecular barriers exhibiting an excellent energy-efficient barrier membrane, suggesting promising permeation characteristics. MXene contains nanochannels that allow the molecules to penetrate through for what is known as “molecular-sieving”, which can selectively separate large compounds, while leading small molecules slip between the channels. MXene membranes have shown superior performance in various separation sciences [6].

The excellent separation performance of MXenes established for their energy-efficient separations due to their structural and chemical variations have led to novel applications even compared to other membrane nanomaterials such as graphenes and zeolites that can separate molecules by physical trapping (or sieving effect) of the molecules in tiny channels and grids like a net. The research efforts in this area have opened-up new windows for the application of membrane separation technology providing higher probability of tailoring the separation performance to a large variety of compounds. In this review, methods of MXene synthesis, MXene membrane fabrication, engineering of MXene membrane nanochannels, and their use in numerous separation arenas are discussed (Fig. 1).

This review is especially devoted to providing an evidence for the fundamental concepts presented in the current state-of-art technologies for preparing 2D MXene-based membranes and the pros and cons of various characterization methods on these 2D membranes are elegantly

---

* Corresponding author.

E-mail addresses: mashalah.rezakazemi@gmail.com (M. Rezakazemi), ahmad.arabishamsabadi@drexel.edu (A. Arabi Shamsabadi), haiqingl@buffalo.edu (H. Lin), patricia.luis@uclouvain.be (P. Luis), aminabhavit@gmail.com (T.M. Aminabhavi).

[1] The authors contributed equally to this work.

https://doi.org/10.1016/j.rser.2021.110878
Received 6 October 2020; Received in revised form 19 February 2021; Accepted 24 February 2021

detailed. A rather comprehensive in-depth study was carried out to investigate which modifications would be beneficial to utilize 2D MXene-based membranes. Furthermore, the physicochemical properties of the applied membranes will appeal to the materials science community by addressing the production methods of 2D MXene separation membranes with enhanced permeation and separation properties.

2. MAX phase and MXene structures

MAX phases are organized with the general formula: $M_{n+1}AX_n$($n = 1$–3) where M is an early transition metal (i.e., Ta, Hf, Mo, Nb, Zr, Mn, Cr, V, Ti, Sc), A is an A-group element (Cd, Al, Gl, In, Tl, Si, Ge, Sn, Pb, P, As, Bi, S), and X is carbon and/or nitrogen. The MAX phases are the layered hexagonal compounds (space group $D^4{}_{6h}$–$P6_3$/mmc) with two formula units per unit cell. The structure of a MAX phase consists of the close-packed layers of M atoms that are interleaved with A-element layers in the center of the trigonal prism, where X elements fill the octahedral site in M_6X. Their respective chemistry also categorizes these phases based on the value of n: “413” for M_4AX_3 ($n = 3$), “312” for M_3AX_2 ($n = 2$), and “211” for M_2AX ($n = 1$) [11].

MXenes are formed by selective eliminating Al from MAX phases. MXenes consist of transition metal carbides and either carbonitrides or nitrides with layered-structures with the general formula: $M_{n+1}X_nT_z$ (where T corresponds to the surface functional groups such as F, O, H and OH). The thickness of individual MXene flakes is commonly below 1 nm, whereas the lateral size of MXenes varies from nanometers to micron size during the synthesis (Fig. 2D).

3. Preparation methods and modification approaches

Various MAX phase synthesis methods have been established over the past decades such as self-propagating high-temperature synthesis (SHS), chemical vapor deposition (CVD), combustion synthesis, arc melting, physical vapor deposition, hot isostatic pressing (HIP), spark plasma sintering (SPS), reactive sintering, and mechanical alloying. In all these methods, MAX phases are synthesized either via the bottom-up or top-down methods [12]. Furthermore, the surface can be modified to enhance the separation performance of MXene-based membranes. Hence, the general synthetic route of MXene nanosheets as well as their surface modifications are comprehensively reviewed in this section.

3.1. Top-down synthesis methods

As MXenes have layer-by-layer structures similar to the bulk precursors of other 2D nanomaterials, the conventional exfoliation techniques such as a top-down synthesis method can be employed to fabricate the MXene nanosheets. The exfoliation approaches are commonly based on the cleavage of relatively large bulk precursors through the MAX-phase or non-MAX-phase using etching agents or intercalants.

3.1.1. Precursor: exfoliation based on MAX-phase

In MAX phases, the bond between M and A atoms is mostly metallic; hence, for producing MXenes, it is difficult to separate $M_{n+1}X_n$ layers by mechanical shearing method. Since the M–X bonds are stronger and less chemically active than the M–A bonds, etching of A-atom layers is selectively conceivable. In this method, highly selective etching is the heart of the MXenes synthesis protocol. However, MXene is commonly produced via selective etching of a MAX phase (which is selected based on the targeted MXene), mostly by utilizing the robust etching reagents consisting of a fluoride ion (F^-) such as hydrofluoric acid (HF) [13], ammonium fluoride (NH_4F), ammonium bifluoride (NH_4HF_2), a mixture of hydrochloric acid (HCl) and lithium fluoride (LiF), and a mixture of HCl and HF [14] (Fig. 2A and B). Depending upon the objective, MXene and different MAX-phase precursors with the general formula: $M_{n+1}AX_n$(MAX) are available. MAX-phases containing Al ($M_{n+1}AlX_n$), Si ($M_{n+1}SiX_n$), and Ga($M_{n+1}GaX_n$) with various metal compositions are the most common precursors used. In a typical MXene synthesis process, by etching the MAX phase precursors (i.e., Ti_3AlC_2 or Ti_2AlC) in an etching solution (HF or acid-fluorides) at ambient temperature, the MXene stacks (Ti_3C_2 or Ti_2C) are allowed to adhere to each other. This process selectively removes the Al (A) species and terminates the carbide layers surface by –OH, –F, and –O–groups (Fig. 2E and I). A single-layer (or multi-layer) stack is then selectively obtained by the etching of glue-like ionic bonding layers (Fig. 2G and H). Indeed, the precursors are first treated with an etching solution, which are then sonicated or imposed to shearing forces to achieve single-layer MXene stack (Fig. 2B) [15].

3.1.2. Precursor: exfoliation based on non-MAX-phase

MXene can also be synthesized from non-MAX-phase precursors. For instance, zirconium-containing carbide ($Zr_3C_2T_z$) MXene was fabricated by selectively etching Al_3C_3 from the non-laminated $Zr_3Al_3C_5$ [21] and Mo_2CT_xMXene by etching Ga from non-laminated Mo_2Ga_2C [22]. The non-MAX-phase precursors are similar to MAX-phase precursors except

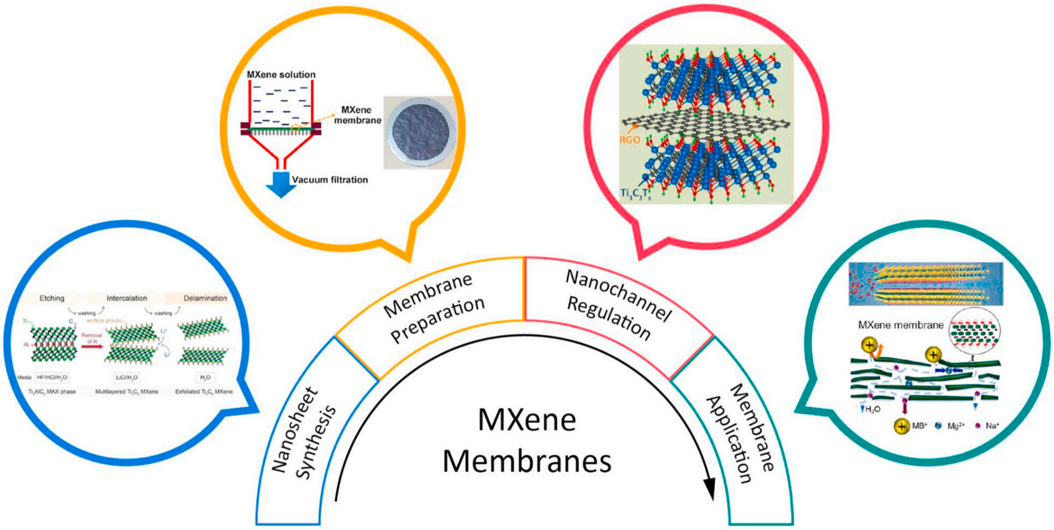

Fig. 1. Overview of MXene membranes (fabrication, nanochannel regulation, and applications). Left to right [6–10].

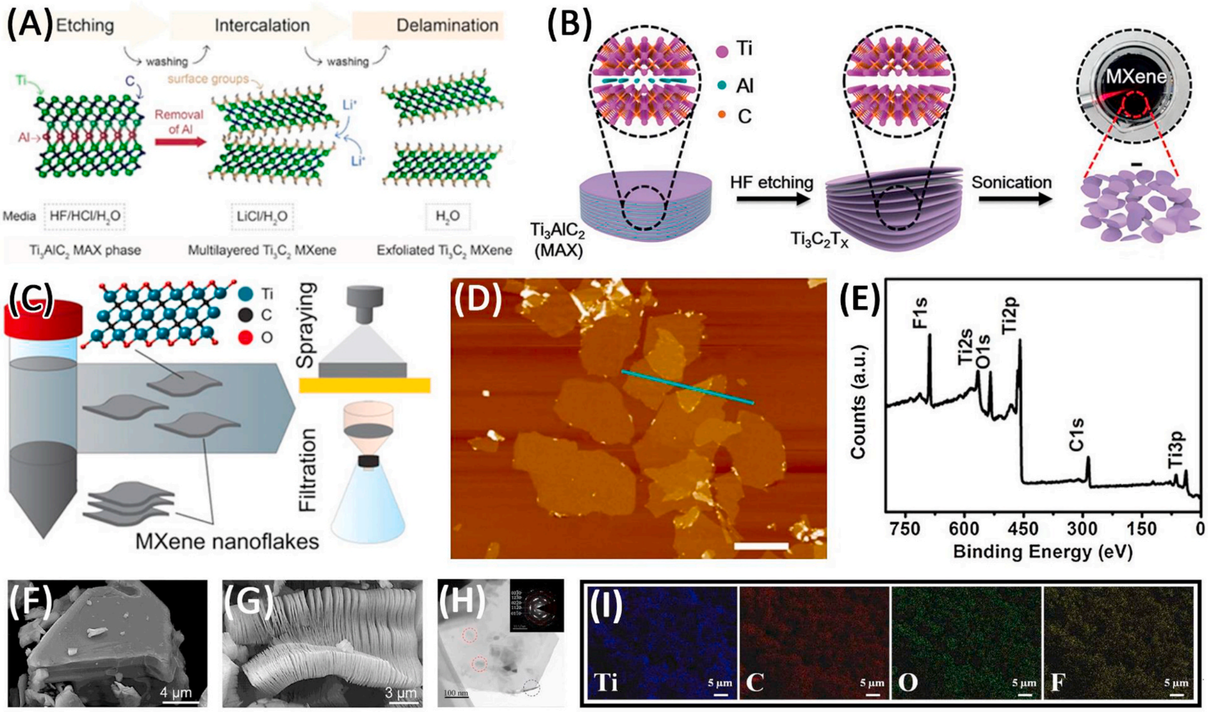

Fig. 2. MXene synthesis, processing, structure and elemental compositions: (A) synthesis of $Ti_3C_2T_z$ MXene using HF/HCl media [7]; (B) synthesis of $Ti_3C_2T_z$ MXene using HF media [16]; (C) $Ti_3C_2T_z$ MXene processing [17]; (D) AFM of $Ti_3C_2T_z$ MXene flakes [6]; (E) XPS survey of $Ti_3C_2T_z$ MXene [18]; (F) SEM of $Ti_3C_2T_z$ MAX phase [2]; (G) SEM of multilayer $Ti_3C_2T_z$ MXene [2]; (H) TEM of $Ti_3C_2T_z$ MXene flakes [19]; (I) EDX of $Ti_3C_2T_z$ MXene [20].

the two A-element layers separate the carbide layers and the A-X units, instead of neat A-element units, which are to be etched to obtain MXene. For example, Al–C layers instead of neat Al-element layers are etched from $Zr_3Al_3C_5$ precursor to obtain Zr_3C_2 [21]; the Ga–C layers are etched from Mo_2Ga_2C to synthesize Mo_2C [22] and Al_3C_3 are etched from $U_2Al_3C_4$ to fabricate U_2CT_x [15]. The $Zr_3Al_3C_5$ has been classified as beyond MAX phases with the generic formula: $MnAl_4C_{n+3}$ and $MnAl_3C_{n+2}$ (where n = 1–3, and M = Hf or Zr) [21]; here, the metal layers are separated by the carbon layers, i.e., Al–C layers separate M_3C_2 or M_2C layers. Indeed, in $Zr_3Al_3C_5$, the etching of Al–C layer is energetically more favorable than the etching of Al-element layers [21].

3.1.3. Exfoliation based on etchants

The exfoliation synthesis approach based on etchants is classified as HF-etching and non–HF–etching methods. HF is an efficient etching reagent, which has been extensively used in chemical research. HF causes MXene stacks to detach from each other by reacting with the attaching metals (Al, Ga or Si) when used as highly concentrated HF [1]. Since HF is a hazardous solvent, so several alternative reagents have been employed. However, using HF has an advantage as it can be generated either by *in-situ* formation or by reacting with an acid such as HCl with fluorides (e.g., NaF or LiF) or by the use of molten fluorides at elevated temperatures. In case of the latter, the free fluoride ions (F^-) might corrode the attaching metals (Ga or Al).

MXenes can also be synthesized using fluorine-free mechanical force assisted liquid exfoliation approach using ultrasound probe sonication followed by bath sonication in the presence of an intercalant [23]. More lately, Ti_3C_2 MXene was synthesized using ultrasound in the presence of tetrabutylammonium hydroxide (TBAOH) intercalant [15] and the terminal groups on the surface of MXene were determined by the etchants. For example, etching with a fluorine-containing etchant generates plenty of –F groups on MXene surface, thereby decreasing the amounts of other functional groups such as –O–and–OH.

The exfoliation synthesis approach based on the delamination of intercalants is classified as metal-ion and intercalant-organic intercalants. In the multilayer MXenes, the stacked T-functionalized titanium carbide MXenes ($Ti_{n+1}C_nT_x$, where T = F, O, and OH) have the binding energy of stacked MXene up to about 2–6-times more than that of the bulk MoS_2 or graphite having weak interlayer interactions. However, to achieve improved exfoliation of MXene into monolayers with a binding energy of 1.0–3.3 J/m^2 requires more weakening of the interlayer interactions [24] and thus, the conventional mechanical exfoliation methods are not applicable for the successful synthesis of single-stack MXenes. Therefore, various delamination intercalants are used before inducing the mechanical stresses (such as high-speed mixing and sonication) to exfoliate the etched MXene precursors. For example, metal-ion intercalants such as metal hydroxides or halide salts were used to delaminate the large-size MXenes. Intercalant-organic intercalants were also used such as large organic base molecules (e.g., n-butylamine, TBAOH, choline hydroxide, tetrapropylammonium hydroxide (TPAOH)) as well as polar organic molecules (e.g., dimethyl sulfoxide (DMSO) and isopropylamine) [25,26].

3.2. Bottom-up synthesis methods

The bottom-up preparation methods often utilize small inorganic or organic elements/species, which are assembled into a 2-D ordered structure via the crystal growth. These methods have the benefit of accurate manipulation of morphology, surface termination, and size distribution of MXenes. In comparison with other 2D nanomaterials, the available proposed bottom-up preparation approaches of MXene are yet to be successful, presumably because of the existence of multi-component element layers in the MXene. Ren et al. [27] prepared high-quality large-area 2-D ultrathin α-Mo_2C crystals at temperatures higher than 1085 °C by the CVD method under CH_4 environment as a carbon source onto the Cu/Mo support, since Cu and Mo would form a metal alloy at such elevated temperatures. In addition, Mo penetrates into the alloy surface to react with the carbon source to form an α-Mo_2C crystal with an orthorhombic structure and lateral sizes up to 100 µm and a few nanometers in thickness. The CVD method can also be used to synthesize TaC and WC crystals from the other 2-D transition metal carbides, such as Ta and W [27]. This approach provides MXene with fewer defects and sizeable lateral sizes. However, the bottom-up CVD method could produce a homogeneous, few atomic thin layer and large area MXene without surface terminations.

It may be noted here that the bottom-up preparation approach has faced with a major challenge for the monolayer MXenes stack as finding a solution is a major challenge. The small element/species precursors in comparison to the bulk precursors may have the possibility to tune and formulate the morphology, surface termination, composition, and growth of MXenes. However, surface termination induces a remarkable effect on the performance of MXenes that is less adjustable throughout the top-down preparation methods (often imposing a complex combination of terminations). While certainly the terminal groups are more or less fixed during top-down synthesis, but given the rich chemistry, MXenes can be easily functionalized to give tailored functional groups for targeted applications. Hence, to examine the inherent characteristics of MXenes, an accurate determination of surface terminations is necessary. Consequently, an indispensable orientation for the expansion of bottom-up preparation approaches is greatly favorable to achieve MXenes with predetermined properties.

3.3. Functionalization and Stabilization of MXenes nanosheets

Different molecules and ions can be incorporated between the layers of MXenes by the intercalation methodology, which can be necessary to exploit nanomaterials' unique properties. The MXenes performance in different applications strongly depends on the termination-mediated surface functionalities. The termination and relative stabilization are originated from the orbital hybridization between the surface elements and the functional groups. Indeed, termination stabilizes MXenes using low-energy orbitals of termination via saturating the nonbonding valence electrons of the surface elements. For example, in $Ti_3C_2T_z$ MXenes, orbitals splitting of surface element (3d orbitals of Ti) shows pseudo gaps, indicating the stabilities that can follow the order: $Ti_3C_2 < Ti_3C_2H_2 < Ti_3C_2(OH)_2 < Ti_3C_2F_2 < Ti_3C_2O_2$ [28]. Therefore, for $Ti_3C_2T_z$, four moieties of termination (C–Ti-O_x, C–Ti-$(OH)_x$, C-TiF_x, and Ti_3C_2OH–H_2O) are possible [6]. MXene flakes due to the synthesis in an aqueous environment can be surface-functionalized with different functional moieties (T_z). Taking into account the wide groups of MXenes, the termination can be practically regulated by configuring the valence electrons via conforming the termination to the *M* element.

The MXenes surface can be generally functionalized via electrostatic attractions, physical adsorptions, and the formation of the covalent bonds. MXenes generally exhibit negative surface charge because of –F and –OH groups on the surface. Hence, a positively charged compound can be attracted onto the MXene surface through the electrostatic attractions. For instance, the positively charged polymers can be adsorbed onto the surface such as poly(vinylpyrrolidone) (PVP) and polyethyleneimine (PEI) [25] and polymers can also interlock the MXene flakes. For example, PEI creates robust electrostatic interactions with MXene dispersion to form improved hydrogen bonded structure with MXene flakes because both oxygen moieties and amino groups may play as the acceptor or donor for the formation of hydrogen bonds [29]. Hence, crosslinking PEI into MXene nanosheets strongly interlocks the nanofilms. Thus, the surface charge of $Ti_3C_2T_z$ MXene can be changed from positive to negative at neutral pH using the silane-coupling agents bonded both physically and chemically [30]. The functionalization allows for in situ fabrication of the self-assembled membranes via the layer-by-layer assembly.

4. Preparation of 2-D MXene-based membranes

A nanofilm with fewer defects is vital for achieving high-performance 2-D-material membranes, whose separation performance is intensively dependent on the stacking configuration and lateral size of the nanosheets [31]. Exfoliated sheets with 1–2 μm in the lateral size are desirable for preparing the ordered 2-D-stacking structures and numerous in-plane gaps for high-throughput separations [32]. MXenes with a wide range of chemistries have thus opened new windows for the next-generation membrane materials seeking newer applications. They are resistant to chemical attack, thermal shock, oxidation, and often creep-fatigue as well as damage-tolerant, readily machinable, and durable (the robust material of its kind) [33].

Vacuum-assisted filtration is a scalable technique to horizontally align MXene flakes onto a support to prepare ultrathin MXene membranes (Figs. 3A–2D). In this method, an MXene colloidal suspension is passed through a porous support under vacuum, where MXene nanosheets build a robust layered MXene membrane (Fig. 3E–H). The MXene membrane can be readily separated from the support and it can be free-standing [6]. This relatively simple a method that can enable the manufacturing-scale production. Fig. 4 shows the scalable synthesis of MXene [34].

5. MXene membranes in separation

As majority of the commercial purification operations are thermodynamically far from the minimum separation, they account for 70% of the total investments of a separation unit [35]. Therefore, with increasing energy costs and enhanced focus on sustainability and efficiency, the development and performance of energy-efficient membrane processes create significant opportunities in different industries ranging from water/wastewater treatment, carbon capture, chemicals refining and production [36,37]. Hence, in order to meet the rising demands, intense interests have been directed towards developing membrane materials with high flux and separation factor [38,39]. In this respect, 2-D nanomaterials [40] including metal-organic frameworks (MOFs) [41–45], zeolitic imidazolate frameworks (ZIFs) [46], zeolites [47], graphene, and graphene oxide (GO) [48] nanosheets have proved to be the promising membrane materials. However, the structure of these nanomaterials (such as MOFs or zeolites) deteriorates during the exfoliation process. Similarly, it is hard to synthesize graphene nanosheets providing with the homogenous and controllable nanopores because their stochastic nature limits the performance on a large scale [49,50]. Graphene is also restricted to just carbon in its composition, while those materials having artificial or intrinsic nanopores on the sheets act as the molecular sieving pathways, such that the 2-D materials can be stacked forming the interlayer channels for the molecular separation [29]. This has prompted more research efforts on developing different types of MXenes as the next separation 2-D materials for membrane applications including those of gas separation, pervaporation (PV), water purification, desalination, wastewater treatment, and heavy metals removal. By changing the T_X, different narrow channels among the adjoining sheets can be built in the stacked MXene laminates for the separation of molecules having different sizes [51].

Despite excellent separation efficacy of MXene membranes, their separation performance decreases upon exposing to air and/or humidity [52]. Effective protocols should be applied to prevent the degradation of MXene membranes [53]. In addition to fundamental research on structural engineering, it is very important to fabricate highly stable MXene membranes having high resistance when they are exposed to water and oxygen. The poor chemical stability of MXenes can be improved if they are incorporated into polymer matrices. MXene/polymer composites have been fabricated using in-situ polymerization or ex-situ incorporation [54–57]. In *in-situ* polymerization, strong covalent bonds can be formed between MXenes and polymers. However, there are a limited number of monomers capable of polymerizing on the surface of MXenes. Ex-situ incorporation has been extensively used to synthesize MXene/polymer composites; it allows for tuning the composition and structure of polymers and preventing MXenes degradation [58].

In the literature, different approaches have been employed for engineering the interlayer gallery of MXenes (Fig. 5). Highly ordered 2-D

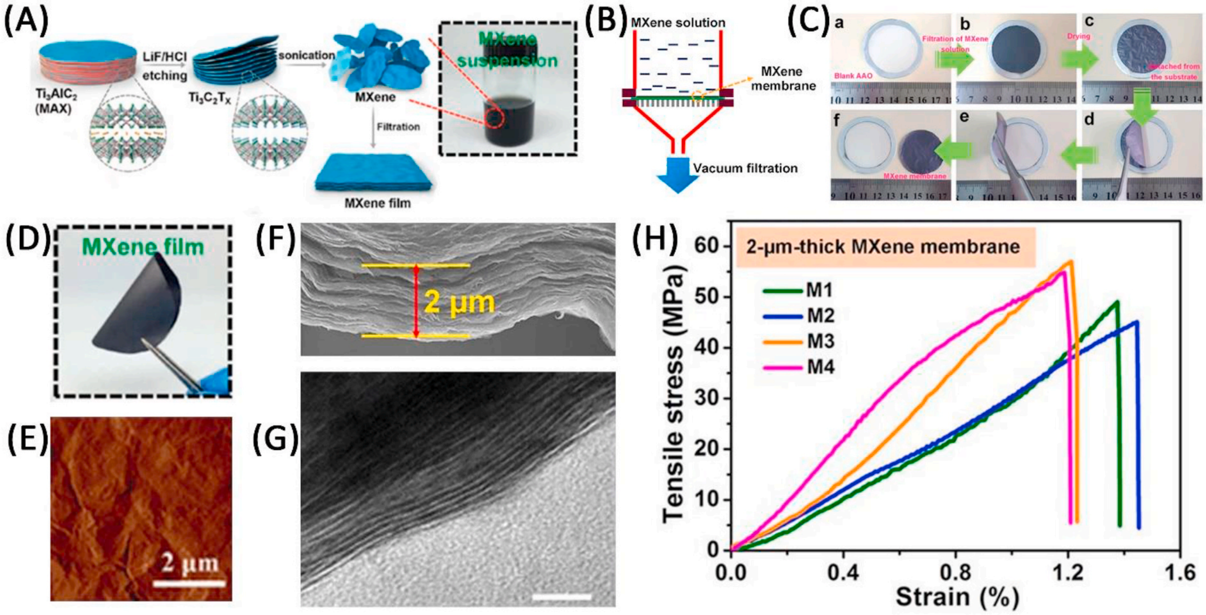

Fig. 3. MXene membrane preparation, structure, and strength: (A) delamination of $Ti_3C_2T_z$ MXene; (B) vacuum filtration [6]; (C) $Ti_3C_2T_z$ MXene membrane procedure [6]; (D) $Ti_3C_2T_z$ MXene membrane flexibility; (E) AFM of $Ti_3C_2T_z$ MXene membrane surface [16]; (F) cross-sectional SEM of a 2 μm $Ti_3C_2T_z$ film [6]; (G) cross-sectional TEM of $Ti_3C_2T_z$ film [6]; (H) mechanical properties of a 2 μm $Ti_3C_2T_z$ MXene membranes [6].

nanochannels can be generated via intercalation of hyperbranched PEI and MXene nanosheets followed by the interfacial polymerization using trimesoyl chloride and 100 nm defect-free MXene membranes were assembled with the regular stacking structures [59]. Sintering and freeze-drying of $Ti_3C_2T_z$ MXene membranes can change the interlayer galleries of the assembled lamellar membranes [60,61]; insertion of other 2-D nanomaterials into MXene layers is another effective strategy to manipulate the interlayer spacing for targeted separations [8].

5.1. MXene membranes in gas separation

Molecular-sieving mechanism in nanoporous membranes with the homogeneous and adequate channels that can surpass the trade-off between the permeability and selectivity are favorable for highly energy-efficient gas separation [63]; in such situations, emerging 2-D nanomaterials would provide novel pathways for the advancement of membrane separation. Concerning the molecular sieving membranes in the form of lamellar, disordered interlayer channels can be produced among the randomly laminated adjoining sheets, which can decrease the selectivity. Hence, the fabrication of laminated membrane with substantially ordered channel is still a challenging task for ultrafast and rigorous gas sieving. However, the lamellar stacked structure of the sheets would influence the separation properties [48]. For example, a randomly stacked GO membrane showed only Knudsen diffusion with a low gas selectivity, whereas an ordered GO membrane showed gas sieving with a highly enhanced selectivity [48]. Furthermore, numerous other ordered laminated GO membranes displayed increased permeability and selectivity in comparison to other disordered membranes [64]. However, since oxygen-functional groups causing the defects in GO nanosheets are not easy to control, since the random laminated structure is often formed in the membranes [64]. Such defects act as active sites for interactions with the gases.

Molecular sieving across the thin nanoporous MXenes is of particular interest in gas separation. The exfoliated lamellar MXene-based membranes have the aligned nanochannels with many surface termination groups on the neighboring sheets, resulting in the superior H_2/CO_2 separation characteristics i.e., H_2 permeability is >2200 Barrer and H_2/CO_2 selectivity is >160, which exceeds the state-of-the-art membranes (Fig. 6A–F) [6]. Interestingly enough, despite the smaller kinetic diameter of CO_2 than O_2 and N_2 and its higher affinity to MXene, CO_2 exhibits lower permeability than O_2 and N_2. CO_2 molecules can be adsorbed into MXene nanochannels by blocking the transport and consequently, decreasing the CO_2 permeability. The gases diffuse through MXene nanosheets mostly by the activated diffusion mechanism as the obtained H_2/CO_2 selectivity is far higher than the Knudsen selectivity. However, the structure of MXene membranes (e.g., intercalating species, interlayer distance) substantially affects gas diffusivity and therefore it may be tuned to promote the gas separation performance [65].

Under vacuum filtration, due to the high aspect ratio of MXene nanosheets, nanochannels (interlayer spaces between parallel nanosheets) and nanoslites (void between nanosheets edges) are formed in the fabricated membranes (Fig. 7). These nanochannels provide diffusion pathways for gas transport. Extending the gas pathways and interlayer spacing of nanochannels allows for different gas permeabilities through the membranes. Despite the smaller kinetic diameter of CO_2 than O_2 and N_2 and its higher affinity to MXene, CO_2 exhibits lower permeability than O_2 and N_2. CO_2 molecules can be adsorbed into MXene nanochannels preferentially which block the transport of the CO_2 molecules. Therefore, in addition to engineering the interlayer spacing of MXene assemblies, other parameters should be manipulated to fabricate CO_2 selective membranes [33].

Embedding MXenes in polymers in free-standing and thin-film composite membranes (Fig. 7) result in higher affinity of the matrix toward CO_2, molecular sieving provided by MXene's galleries, and created more tortuous pathways for gas transport. MXene nanosheets are able to enhance gas permeabilities and selectivities of the corresponding MMMs [33].

MXenes have the potential to provide membranes with higher permeability and equivalent selectivity compared to the existing 2-D MOFs and ZIFs membrane materials (MXene>ZIFs>MOFs with the ratio of 100:10:1). However, MXene-based membranes reveal excellent reproducibility, good mechanical properties, no deterioration, and stable separation performance during long-term continuous separation. These superior separation properties are related to the ordered nanochannels in the lamellar MXenes membranes [6].

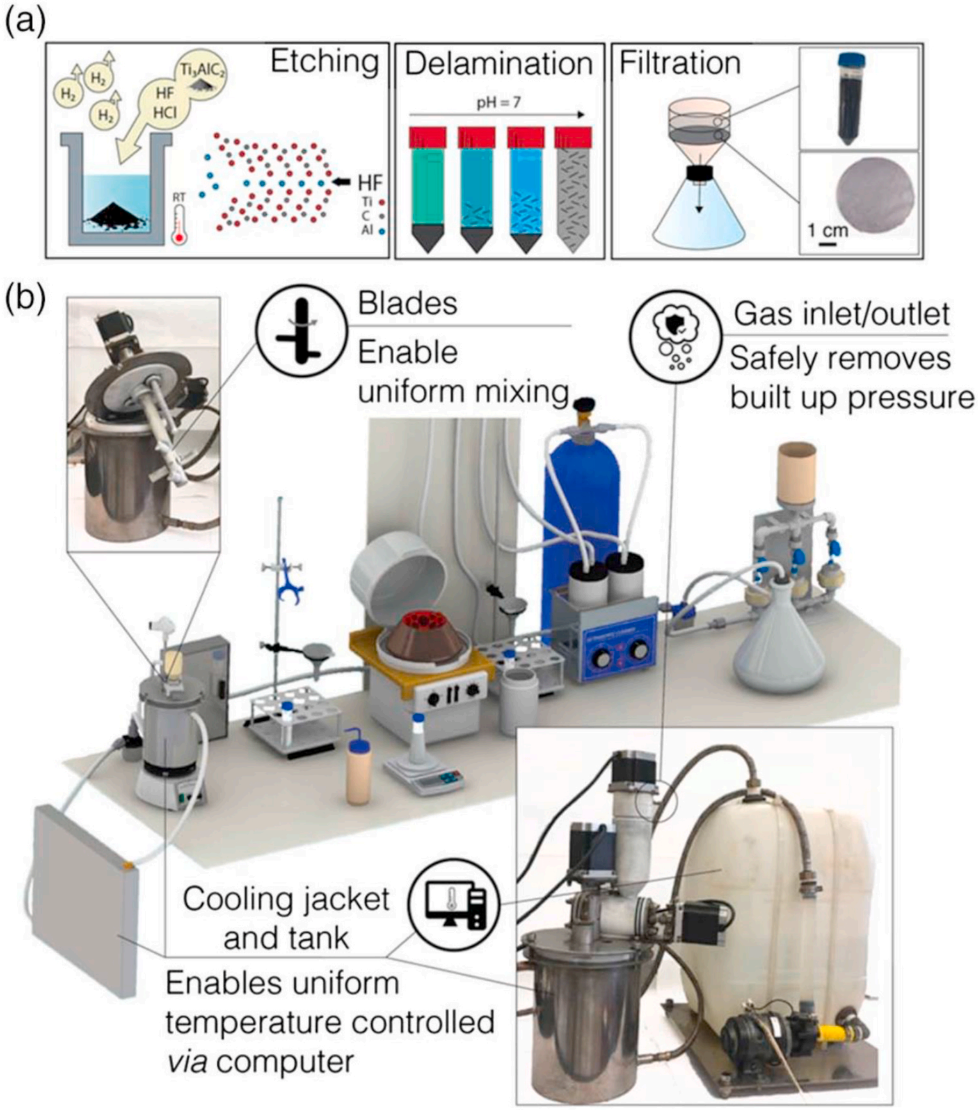

Fig. 4. a) Representation of MXene preparation, b) schematic of MXene large scale reactor and preparation setup [34].

The surface termination of MXene may have a significant effect on the separation properties. However, this effect is not noticeable for $Ti_3C_2F_2$ and $Ti_3C_2O_2$, which showed H_2/CO_2 selectivity of 171 and 200, respectively, presumably because oxygen and fluoride containing groups do not exhibit affinity towards the gas [6]. The orderliness of the channels also has a significant effect on the separation performance. Consequently, a disorder with only 0.1 nm disturbance to the interlayer space would cause low selectivity because the disorder often provides broad slits between the MXene flakes, dramatically decreasing the selectivity. Heating MXene membranes up to 500 °C could shrink their interlayer, reinforcing the molecular sieving properties for hydrogen separation [9].

MXene membranes have a channel size of 0.34 nm and this would be appropriate to differentiate CO_2 (0.33 nm) over N_2 (0.36 nm) or CH_4 (0.38 nm) [6,32]. However, CO_2 molecules can be trapped into the MXenes nanosheets, thereby decreasing the CO_2 permeability. To address this issue, borate was used to crosslink MXene nanosheets. Here, borate not only crosslinks with the oxygen moieties onto the MXene surface in order to reduce the interlayer distance for enhancing CO_2/N_2 or CO_2/CH_4 selectivity, but also leads to reversible reactions with CO_2 to unleash the trapped CO_2 to improve the CO_2 permeability [68]. After crosslinking with borate, the plane-to-plane and in-plane stiffness were reinforced, making MXene sheets hard to be scratched [31] (Fig. 6H). A CO_2 permeance of 350 GPU together with a moderate CO_2/CH_4 selectivity (15.3) were obtained for the functionalized MXene nanofilm. The membrane displayed long-term stability over 100 h. Other functionalizations should be applied to make MXene membranes competitive with state-of-the-art CO_2 separation membranes such as zeolites, MOFs, and microporous polymers [69].

$Ti_3C_2T_z$ can also be embedded in a block copolymer of Pebax the $Ti_3C_2T_z$, resulting in well-formed galleries for a fast and selective CO_2 transport (Fig. 6I) [67]. The embedment of MXene in polymers also mitigates its oxidation. Table 1 shows the gas separation properties of some state-of-the-art membranes used for H_2/CO_2 separation. In same circumstances, MXene membranes show superior separation properties in terms of the selectivity and permeability. The excellent separation properties are related to the nanometer channels in the stacked MXene membrane [6].

For the case with unclear thickness, permeability is calculated by multiplying permeance by thickness of 0.1 μm.

5.2. *MXenes membranes in liquid separation*

Membranes have attracted much interest in liquid separation studies by pervaporation (PV) [88,89], which avoids the liquid-liquid azeotropic composition. Mixed matrix membranes (MMMs) incorporated

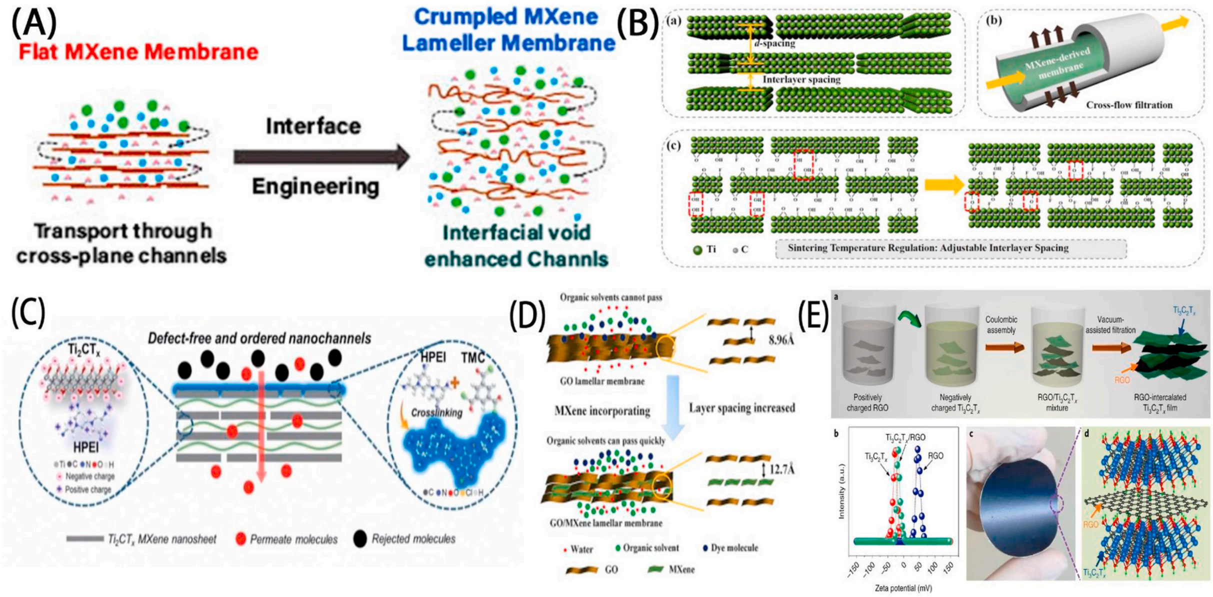

Fig. 5. Engineering of nanochannels in MXene membranes: (A) crumpled MXene lamellar membrane with enhanced interfacial voids [60]; (B) adjusting interlayer space of MXene with sintering [61]; (C) crosslinked Ti_2CT_z MXene membrane [59]; (D) MXene/GO membrane [62]; (E) MXene/RGO membrane [8].

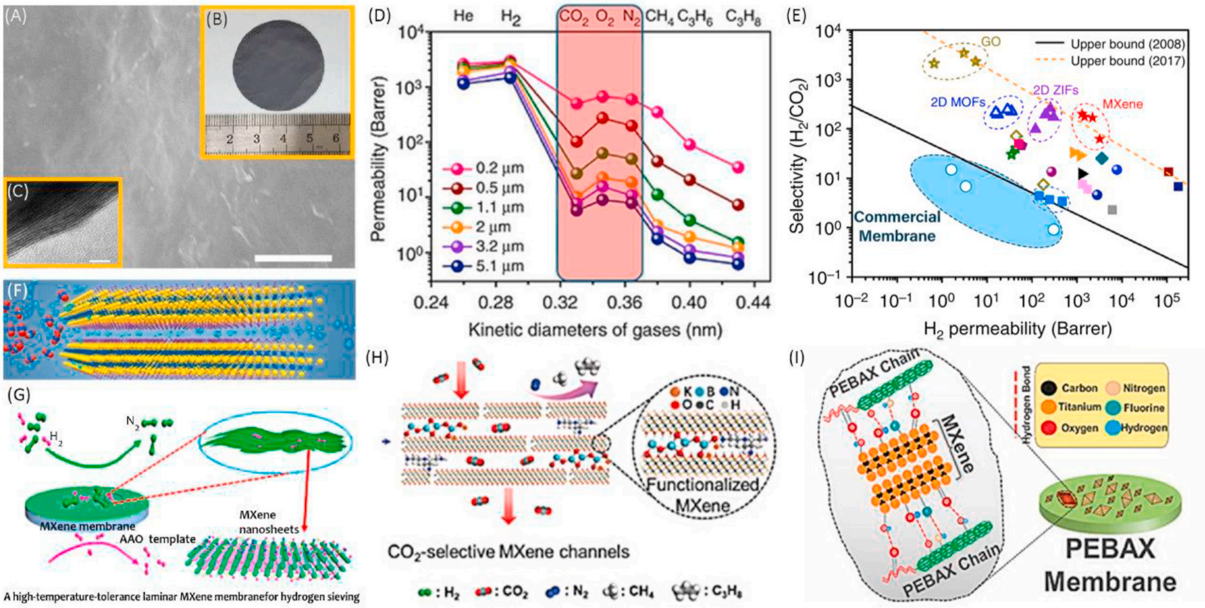

Fig. 6. MXene-based membranes for gas separation: (A) top surface SEM of $Ti_3C_2T_z$ MXene membrane [6]; (B) digital photograph of $Ti_3C_2T_z$ MXene membrane [6]; (C) cross-sectional SEM of $Ti_3C_2T_z$ MXene membrane [6]; (D) permeability of different gases in terms of kinetic diameters [6]; (E) performance of MXene membranes relative to the upper bound [6]; (F) hydrogen separation mechanism of MXene membrane [9]; (G) sintered MXene membranes for hydrogen separation [9]; (H) functionalized MXene membranes for CO_2 separation [66]; (I) interafacial desing of Pebax/MXene membranes [67].

with hydrophilic nanomaterials such as MOFs and GO have demonstrated high permeability and selectivity for alcohol dehydration [90–93]. With hydrophilicity and its 2-D structure, MXene/chitosan (CS)/polyacrylonitrile (PAN) membranes exhibited high water flux (1400–1470 g.m^{-2}.h^{-1}) and dehydration performance for three zeotropic mixtures [94], i.e., water/ethanol, water/ethyl acetate, and water/dimethyl carbonate. Very high separation factors of 4900, 1420, 900 were achieved for the water/ethyl acetate, water/ethanol, and water/dimethyl carbonate mixtures, respectively. The enhanced selectivity is ascribed to the molecular sieving channels provided by the laminated MXene nanosheets in the CS matrix for the fast and selective transport of water molecules, instead of improving the water sorption characteristics [95]. Structural stability of the MXene (3 wt.%)/CS membrane demonstrated excellent structural stability under cross-flow turbulence with a feed rate of 100 L/h at 50 °C. During 1800 min continuous dehydration of the water/ethyl acetate mixture, the water flux and its content in the permeate side were almost constant showing high pervaporation stability of the MMMs.

5.3. MXenes membranes in desalination

MXenes provide a new platform of membrane materials for seawater desalination, partially because MXenes can trap the sunlight energy to purify water with an energy efficiency that is the state-of-the-art

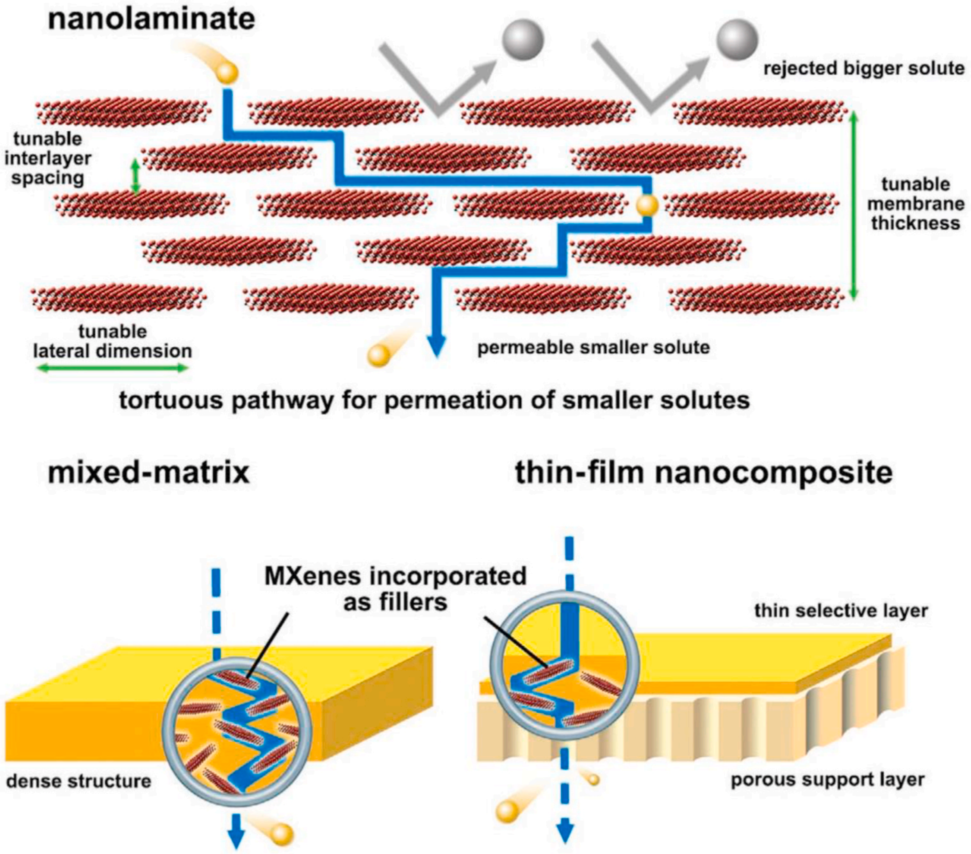

Fig. 7. Separation mechanisms of MXene-based membranes [33].

[96–98]. Ultrathin high-productive and energy-efficient 2-D nanosheet membranes have been used for precise ionic and molecular sieving studies in aqueous solution, demonstrating the potential of these membranes in desalination and water purification studies [99–101]. The interlayer spacings can be widened by intercalating the bulky nanomaterials, crosslinking the massive and inflexible molecules, and encapsulating to enhance the permeability effect [102,103]. Nevertheless, the manipulation of interlayer spacing to separate specific ions is still a challenging area, which impedes the application of these membranes in industrial scales operations [49,104].

The surface functionalities of MXene flakes provide an interlayer spacing in the synthesized MXenes membranes making them suitable for selective separations. Meanwhile, MXenes are hydrophilic and the termination ratio depends sensitively on their preparation methods. The hydrophilic nature of MXenes nanosheets is normally favored for large-scale membrane preparation. For example, MXene membranes have been designed for salt separation based on the hydration radius and ionic charges [10]. A layer of $Ti_3C_2T_z$ MXene was coated onto the polymeric supports using a vacuum-assisted filtration to create the uniform nanochannels with a minimum meso- and macro-pores due to high aspect ratio of MXenes. These membranes exhibited ion sieving and water flux properties that are comparable to GO membranes with the same thickness, while the MXene membrane showed the water flux value 475% higher than the GO membrane [105]. Such an ultrafast water permeation was ascribed [106] to the coexisted water molecules between the layers in the wet condition, thus creating a pathway for water transport. Different physicochemical properties of MXene and GO generate different transport properties to their respective membranes (Figs. 8 and 9C). However, the MXene membranes imped the transport of cations with hydration radii larger than the interlayer gallery, which can sieve single to triple-charge metal and dye cations because of the negative surface charge of MXene adsorbing cations and repelling the anions as verified by the density functional theory (DFT) calculations [105,107]. Different charges of the ions provide various electrostatic interactions by changing the intercalation energy barrier and thereby, the sieving rates [107]. The $Ti_3C_2T_z$-based membranes demonstrated a much better performance than the GO membrane in separating multivalent metal ions, suggesting their potential in practical applications.

Application of external voltage is a promising technique to control the water flux and rejection rates of the MXene-based membranes. For example, MXene membranes can reject NaCl, $MgSO_4$, and methylene blue (MB) [108] (Fig. 9A). Applying a positive voltage decreased the rejection efficiency, but increased the water flux, while applying the negative voltage improved the rejection efficiency, but decreasing the water permeance.

The swelling of MXene membranes can be minimized by the potential interactions between the Al^{3+} and oxygen functionalities onto the MXene surface (Fig. 9B) [115]. These membranes demonstrate an excellent stability and water flux. The surface of MXene can also be modified by the reduction of $AgNO_3$ to Ag nanoparticles (NPs) [114], where MXene was used as a reducing agent as well as a separation layer. The incorporation of NPs has increased the water permeation to nearly four-folds and retained the rejection compared to the nascent MXene membrane. This effect is due to the fact that the NPs might have expanded the interlayer distance and created a short transport path due to extra voids, short water pathways, and improved hydrophilicity of the membranes. The layered NPs/MXene nanosheets exhibited an ultrafast water flux, suitable rejection to model organic foulants, excellent rejection to multivalent ions, and outstanding reusability, all which make them the ideal candidates for NF filtration studies in water treatment. The lamellar structure of MXene membrane provides the transport paths, leading to a very high water flux [51]. However, to promote the water flux of MXene membrane to more than 1000 L m^{-2} h^{-1} bar^{-1}, $Fe(OH)_3$ NPs were used to expand the interlayer distance and to create a

Table 1

Gas separation properties of state-of-the-art membranes used for H_2/CO_2 separation [6].

Membrane Material	Thickness (μm)	Temp. (°C)	H_2/CO_2 Ratio	Permeability (Barrer)	H_2/CO_2 Selectivity	Ref.
Si 400	0.03	200	50/50	179.1	7.5	[70]
Si 600	0.03	200	50/50	44.8	71	[70]
Silicon Carbide	2	200	N.A.	53.1	50	[71]
ZSM-5/Silicalite	9.5	450	50/50	3581.5	25.3	[72]
CMS	N.A.	25	N.A.	300.0	0.92	[73]
CMS	N.A.	25	N.A.	1.6	15	[73]
PBI	N.A.	35	50/50	2.9	7.1	[74]
CAU-1	4	25	N.A.	1289.6	12.3	[75]
ZIF-8	6	30	50/50	2829.9	4.6	[76]
ZIF-7	2	220	50/50	271.6	13.6	[77]
KUUST-1	60	25	50/50	179104.5	6.8	[78]
SIM-1	25	30	N.A.	6119.4	2.3	[79]
COF-MOF	97.2	25	N.A.	110000.0	13.5	[80]
GO	0.0018	20	50/50	0.67	2100	[81]
GO	0.009	20	50/50	3.1	3400	[81]
GO	0.018	20	50/50	5.6	2300	[81]
GO	0.003-0.01	130	N.A.	~35	~30	[82]
GO	0.003-0.01	140	N.A.	~44	40	[82]
ZIF-8/GO	20	250	50/50	~7761.2	14.9	[83]
EFDA−GO	N.A.	25	50/50	840.0	33	[29]
EFDA−GO	N.A.	25	50/50	1200.0	29	[29]
1T MoS2	1	25	50/50	1329.0	7.6	[84]
2H MoS2	1	25	50/50	1740.0	6	[84]
MoS2	0.017	35	50/50	466.5	3.4	[85]
MoS2	0.035	35	N.A.	246.5	3.7	[85]
MoS2	0.06	35	N.A.	146.8	4.4	[85]
2D ZIFs	N.A.	25	50/50	302.0	172	[86]
2D ZIFs	N.A.	25	50/50	194.7	191	[86]
2D ZIFs	N.A.	25	50/50	254.6	261	[86]
2D ZIFs	N.A.	25	50/50	206.0	216: 191	[86]
2D ZIFs	N.A.	25	50/50	119.6	98	[86]
2D MOFs	0.04	20	50/50	28.6	245	[87]
2D MOFs	0.04	40	50/50	35.2	225	[87]
2D MOFs	0.04	20	20/80	31.6	167	[87]
2D MOFs	0.04	20	50/50	15.7	215	[87]
2D MOFs	0.04	40	50/50	17.2	194	[87]
MXene	1.1	25	50/50	3202.3	62	[6]
MXene	2	25	50/50	2226.6	167	[6]
MXene	3.2	25	50/50	1473.3	174	[6]
MXene	5.1	25	50/50	1302.7	200	[6]

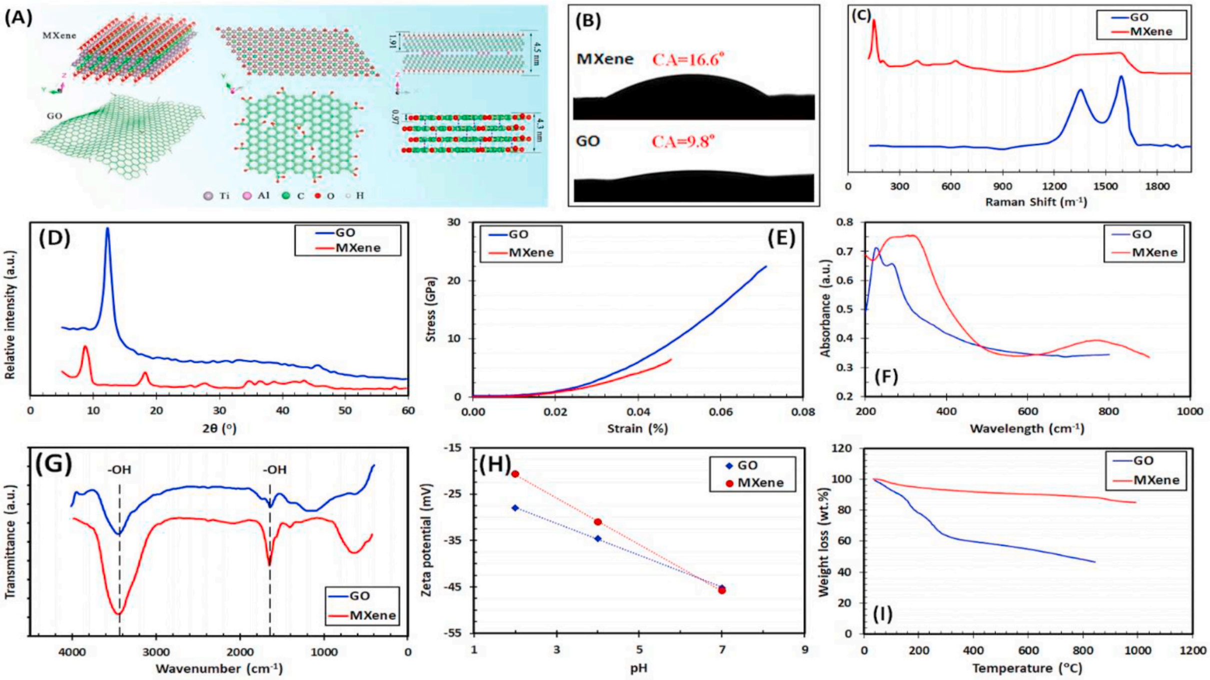

Fig. 8. Physicochemical properties of MXene and GO: (A) molecular structure [16]; (B) contact angle [16]; (C) Raman spectra [109]; (D) XRD patern [16]; (E) mechanical properties [16]; (F) UV–vis spectra [110]; (G) FTIR spectra [16]; (H) zeta potential [16]; (I) TGA thermograph [111].

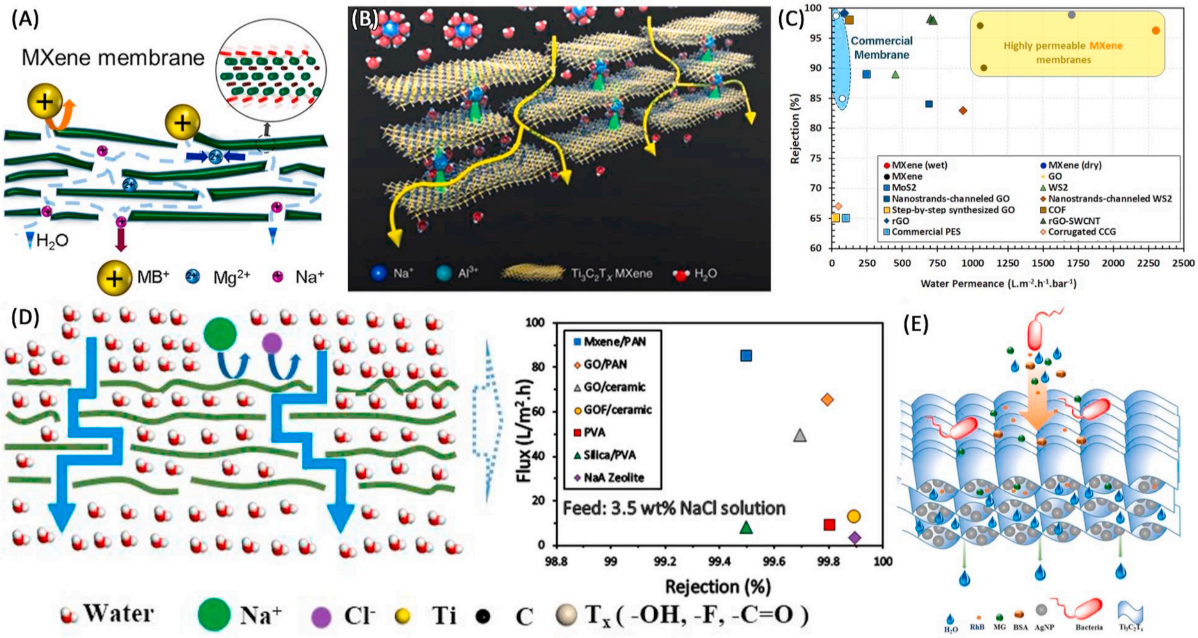

Fig. 9. MXene-based membranes in liquid separation: (A) dye and ion removal ability of MXene membranes [10]; (B) intercalated MXene membranes in water treatment [112]; (C) performance of MXene membrane compared to other membranes in water purification; (D) desalination mechanism of MXene membranes [113]; (E) antibacterial Ag-doped nanofiltration MXene membranes [114].

short transport path. The synthesized MXene can be delaminated by sonication followed by expanding the nanochannels via adding the positively charged $Fe(OH)_3$ suspension to intercalate with the MXene nanosheets. After the deposition on an anodic aluminum oxide (AAO) substrate, the $Fe(OH)_3$ NPs were removed by HCl treatment to give the membranes with outstanding water permeance properties (the highest among the other 2-D materials onto the porous supports) along with very high rejection rates (Fig. 9C).

MXene membranes have also been explored in desalination studies by tuning their structures, surface chemistry, and hydrophilicity. For example, an ultra-thin lamellar $Ti_3C_2T_z$ MXene membrane exhibited the highest water flux reported to date together with an excellent salt rejection rate (Fig. 9D) [113]. This type superb performance of the membrane is attributed to its high hydrophilicity as well as the selective interlayer transport pathways.

5.4. MXenes membranes as power osmotic generators

A massive volume of energy dwells where the rivers meet the ocean. Harvesting such renewable energy (oriented from salty and freshwater mix) needs nanoporous membranes, which could tune the ions flow. Harnessing electrical energy from saltwater may encounter 20% of the world's energy demands. One large-scale technique for this purpose is that of reverse electrodialysis (RED) that utilizes nanomembrane to detach negatively and positively charged ions, producing an electrical energy. However, this is not practical at the pilot-scale, partially due to the expensive semipermeable nanomembranes with tiny nanopores that are simply clogged by bacteria and impurities. However, the stacked negatively charged ultrathin sheets of MXenes lead only positive ions through the maze-like channels, making it an attractive membrane nanomaterial for RED. Tailoring the size of the nanoconfined channels and the surface charge of the ultrathin nanosheets are selective whether cations or anions penetrate through such that charges are specifically separated to produce the electrical energy.

Ion-selective membranes from a lamellar $Ti_3C_2T_z$ MXene are synthesized as high-performance nanofluidic osmotic power generators [116] to attain high-power density up to 21 W/m^2 with an energy conversion efficiency of 40.6% by controlling the charges of the surface at nearly 1000-fold salinity gradient. This density is comparable to today's polymeric RED membranes (Fig. 10). Although other single-layer membranes with single nanotubes or with nanopores have higher power density, the MXene is a much better practical nanomaterial for scaling up applications. MXene membranes can also be synthesized at large-scale [34] using roll-to-roll coating [117] or spray deposition techniques and these can be a cost-effective methods to harvest the electrical energy from the salinity gradients [116]. State-of-the-art polymer membranes costing around \$50 per m^2, while MXene-based membrane might be available at less than half that price [118]. Therefore, the ion-conducting membrane synthesized from MXene might reduce the cost of producing electrical energy from seawater. Table 2 shows energy conversion performances of some state-of-the-art membranes. The MXene membranes shows and higher energy conversion efficiency and higher output power density than most of the state-of-art membranes [119].

5.5. MXenes membrane for wastewater treatment

Dyes solubility in water and living tissues would cause severe health problems due to their toxicity and carcinogenicity. Dye removal from the aqueous solutions is therefore a much-needed effort from an environmental viewpoint as well as to compensate for water scarcity and prevent human diseases related to effluents contaminated drinking water sources. In this area, MXene/polyethersulfone (PES) membranes are known to exhibit high rejection to Congo red dye and Gentian violet [130]. Thus, by regulating the concentration of MXene, MXene-TiO_2 mesoporous membranes can be fabricated on α-Al_2O_3 hollow fiber substrates via dip-coating method [131]. Uniform deposition of TiO_2 NPs onto MXene would result in fine-tuned MXene-TiO_2 layers with longitudinal-lateral transport nanochannels impeding the transport of dextran molecules. However, by increasing the MXene concentration in the coating solutions, the rate of rejection of dextran would increase. The MXene-TiO_2 hollow fiber membranes have shown superior pure water flux. Table 3 shows separation properties of various membranes. As can be seen, the MXene membrane in comparison with other 2D structured membranes such as WS2, MoS2, GO, and other nanomembranes, shows superior separation performance under same

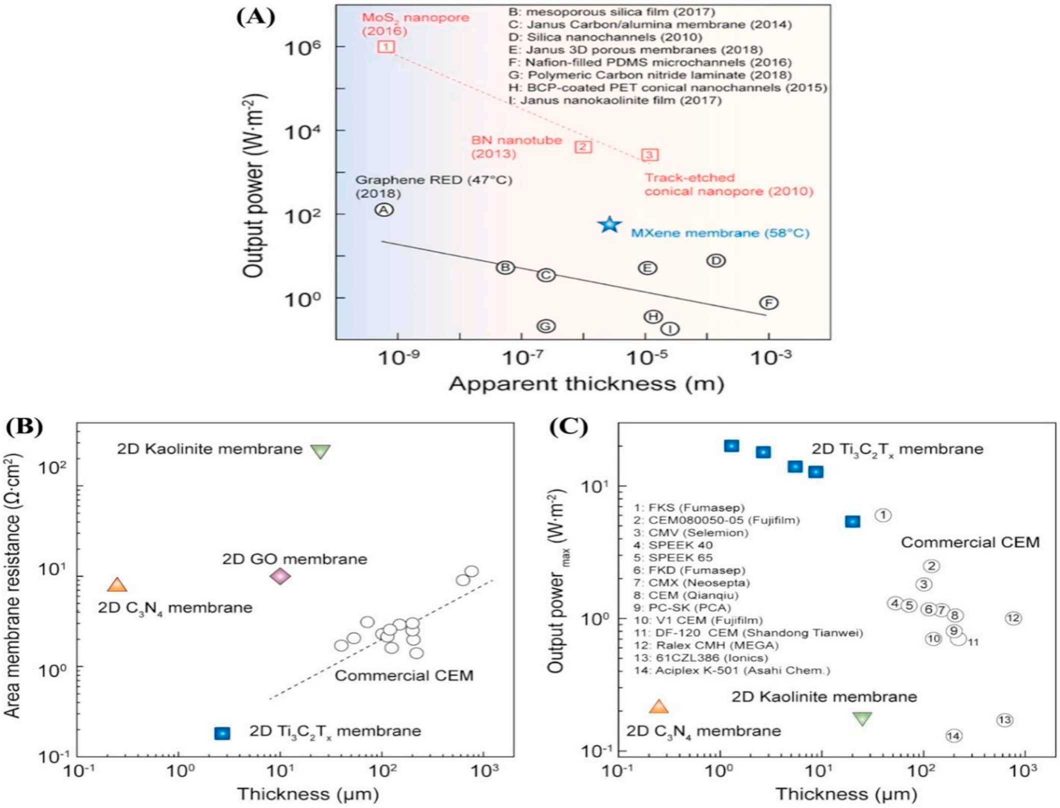

Fig. 10. (A) Power generation performance of MXene membranes compared with the state-of-the-art nanostructured osmotic power generators; (B) Area membrane resistances of various 2-D membranes vs thickness; (C) Osmotic output power density with various thicknesses for different 2-D membranes [116].

Table 2
Energy conversion performances of some state-of-the-art membranes [119].

Membrane	Salinity gradient	Efficiency (%)	Pmax ^{W} $^{-}_{m}$2	Ref.
2D kaolinite	100	44.2	0.18	[120]
Silica nanochannels	1000	31	7.7	[121]
Mesoporous Silica Thin film	10,000	5.05	5.22	[122]
Nafion-filled PDMS micro-channels	2000	36	0.75	[123]
Silk-based hybrid membranes	0.5 M/0.01 M NaCl	17.2	2.86	[124]
GO membrane	0.5 M/0.01 M NaCl	36.6	0.77	[125]
Polymeric-C3N4	0.1 M/0.1 mM KCl	10.2	0.21	[126]
Janus 3D porous membrane	0.5 M/0.01 M NaCl	35.7	2.66	[127]
Polymer/MOF	0.5 M/0.01 M NaCl	29.7	2.87	[128]
Ionic diode membrane	0.5 M/0.01 M NaCl	37.3	3.46	[129]
MXene/Kevlar nanofiber composite	0.5 M/0.01 M NaCl	~20	3.7	[58]
Oppositely charged Ti3^{C}2^{T}x MXene membranes	0.5 M/0.01 M NaCl	44.3	4.6	[119]

conditions. While some membranes exhibit more than 98% rejection rate, the water permeance is less than 100 Lm^{-2}h^{-1}bar^{-1}. The MXene membrane exhibit an acceptable rejection rate and a very high water permeance compared to other membranes [51]. Rejection rates are heavily influenced by the concentration of the solutes due to concentration polarization effect.

5.6. *MXenes membranes with Antibacterial Properties for wastewater treatment*

The available antibacterial agents have negative side effects such as generating toxicity, allergy, and other harmful reactions to humans. Additionally, high microbial resistance has been a stimulus to design new antimicrobial agents providing high activities [141–143]. Using the biocidal nanomaterials has been a promising approach to address these problems for numerous applications such as food storage, desalination, and textile industry. Silver-based NPs [144], 2-D nanomaterials [145], and MOFs with outstanding antibacterial activities have received much attention in recent years [146]. In this venture, highly biocidal MOFs containing antibacterial metals and numerous organic linkers have been developed [147]. However, their reactions with water and linker displacement by aqua ligands make them unsuitable for antimicrobial applications [148,149]. On the other hand, antibacterial activity of GO is governed by the physical and chemical parameters [150].

Recent studies have also demonstrated excellent antimicrobial activity of MXene against Gram-negative [*Escherichia coli* (*E. coli*)] and Gram-positive [*Bacillus subtilis* (*B. subtilis*)] bacterial pathogens [151, 152]. High hydrophilicity of MXene nanosheets could facilitate their effective attachment to bacteria, resulting in bacterial inactivation. Here, the high conductivity of MXene may help to generate a conductive linkage over the shielding lipid bilayer, transferring an electron from intracellular components to the surrounding ensuing in bacteria death. Furthermore, the hydrophilicity of MXene and possible hydrogen bonds between the lipopolysaccharide strings of the cell membrane and MXene surface groups would increase the bacteria/MXene contact and destroying the bacteria [25].

MXenes also demonstrated the potent antibacterial activity in a thin-film form (micron-sized MXene film coated on a PVDF support) [153]. Compared to pristine PVDF, fresh MXene films exhibited bacterial cell viability loss against *E. coli* and *B. subtilis*. Furthermore, aged MXene

Table 3
Separation properties of various membranes for dye removal [51].

Membrane	Thickness (μm)	Application	Dye Concentration	Water Permeance (L m^{-2} h^{-1} bar^{-1})	Rejection (%)	Ref.
GO	2	Evans blue	-	71	85	[132]
MoS2	1.8	Evans blue	15 μM	245	89	[133]
WS2	0.5	Evans blue	15 μM	450	89	[134]
Nanostrands-channeled GO	2	Evans blue	1.5 mM	695	84	[135]
Nanostrands-channled WS2	0.5	Evans blue	15 μM	930	83	[134]
SWCNT-intercalated GO	0.04	Cytochrome c	125 mg L^{-1}	700	98.3	[136]
ZIF-8/PSS	-	Methyl blue	100 mg L^{-1}	26.5	98.6	[137]
F127/PES-80%	-	Alcian blue	0.1 mg L^{-1}	17.6	95.7	[138]
PVDF-SAN-60	-	Congo red	500 mg L^{-1}	9.5	97.7	[139]
MgSi@RGO/PAN	-	Chrome blue-black R	-	4.2	95.2	[140]
Commercial PES (30 KDa)	-	Gold nanoparticles (Dia 5 nm)	500 ppm	100	65	[51]
MXene	0.4	Evans Blue	10 mg L^{-1}	1084	90	[51]
MXene	0.4	Cytochrome c	20 mg L^{-1}	1056	97	[51]

membrane (exposed to air for 30 days) inhibited the growth of both the bacteria because of the synergetic effect of MXene and the formation of free radicals from TiO_2 and defective 2-D carbon structure. MXene membrane exhibited hydrophilicity similar to GO, but it had much higher conductivity (240,238 S/cm) than GO (6.8×10^{-8} S/cm), thus providing more antibacterial potentiality for MXene film [25]. To improve the antibacterial activity of MXene film, silver NPs can be generated on the MXene nanosheets. Compared to the control, 21% Ag@MXene composite membrane exhibited higher *E. coli* growth inhibition (Fig. 8E) [154]. In addition to MXene, strong antimicrobial activity of Ag@MXene composite membrane can be ascribed to the positive synergetic effect of Ag NPs and TiO_2 NP_S produced onto the surface of the nanocomposite during self-reduction of silver nitrate to Ag NPs. Imposed stress on the bacteria cell membrane led to membrane rupture, and thereby, bacteria growth inhibition. The difference in surface functional groups, surface charge, transition metals, C and/or N, and several layers may endow various toxicity levels to MXenes that should be further investigated.

6. Current challenges and future directions

Extensive developments in the separation science areas of MXenes are the result of fabrication of a variety of structural entities that can be synthesized by chemically etching out the layers from the layered materials. This method creates a sponge-like structure having the slit pores of different sizes. Therefore, rationally tuning the structure of 2-D nanochannels could highlight the tracking of MXene nanomaterials for suitable molecular separations with the adaptable functionalities. However, advances in developing improved MXenes have faced with two significant “bottlenecks”: (i) lack of techniques for adjusting the distances of the nanochannels into the MXenes flake and (ii) lack of procedures for practically fabricating the mechanically robust, tear- and crack-free, large-area membranes. Recent breakthrough has solved both these issues as the distance of nanochannels in a $Ti_3C_2T_x$ MXene can be predetermined using Ti_3AlC_2 MAX phases and following the etching procedures. The nanochannels can be formed in a manner, which keeps them chemically active, thereby they would trap particular species during transport through the matrix. Delamination method which can synthesize MXene monolayer with sizeable lateral dimensions still require extra improvement [155]. As a consequence, MXene membranes perform better than most of the similar types of membranes.

Furthermore, it is necessary to focus on how to efficiently process different types of MXenes to achieve excellent stability. The oxidation of MXenes is fastest in the presence of water and slowest in solid media (including polymer matrices) [156,157]. Hence, the preparation of membranes based on MXenes remains still a challenging task as they are vulnerable to chemical degradation by oxidation. However, a high-throughput of feasible structures for MXenes offers researchers much needed valuable directions for selecting the best candidate out of the various probable nanomaterial recipes. On the other hand, the common ‘first principles’ determination methods are numerically too severe for such a study to be practical.

Current research efforts concerning MAX phases as well as MXene membranes are moving in many directions. More efforts are being devoted toward the preparation of novel MAX phases in the bulk as well as thin film forms and their composites. At any rate, before the best MXene can be recognized for separation applications, the principles of chemistry and physics of these nanomaterials should be well understood and the preparation-structure-property relationship should be established to make MXene realize its true potential. The newer methods to synthesize crack-free MXene flakes will be a high priority in sensing the best separation properties of the atomically thin MXene membranes for a wide range of separation applications including hydrogen recovery, carbon capture and water or wastewater purifications. Furthermore, fabrication of MXene-based membranes to compensate reverse selectivity of CO_2/N_2 is of great importance.

The conventional technique for the preparation of MXenes using dangerous HF is accompanied by critical environmental and health concerns. The substitution of HF with less toxic [158,159] or green etchant could guarantee an environment-friendly method for the MXenes preparation. Some efforts have been conducted to replace HF with less toxic or green etchant. However, more consideration is needed in this area. Moreover, the trouble in the preparation of MXenes with homogenous and neat surface termination is another problem in the hands-on applications [97].

Another challenge in MXenes preparation is the low yield [143]. Presently, MXenes are mostly synthesized at the lab-scale with a low yield. Producing large-scale MXenes with an environment-friendly, cost-effective, and efficient will has received more attentions in this area and shall create a new window of producing MXenes at commercial scale [34,97]. Selection of MXenes for fabricating pristine and hybrid membranes begins with estimation of transport properties of the corresponding membranes and identification of mechanisms for both gas, liquid, molecules, and ions transport. Experimental diffusion and adsorption analyses and molecular simulations are options to pursue these goals.

Declaration of competing interest

The authors declare that they have no known competing financial interests or personal relationships that could have appeared to influence the work reported in this paper.

References

[1] Naguib M, Kurtoglu M, Presser V, Lu J, Niu J, Heon M, et al. Two-dimensional nanocrystals produced by exfoliation of Ti3AlC2. Adv Mater 2011;23:4248–53.
[2] Naguib M, Mashtalir O, Carle J, Presser V, Lu J, Hultman L, et al. Two-dimensional transition metal carbides. ACS Nano 2012;6:1322–31.

[3] Chen J, Huang Q, Huang H, Mao L, Liu M, Zhang X, et al. Recent progress and advances in the environmental applications of MXene related materials. Nanoscale 2020;12:3574–92.

[4] Gogotsi Y, Anasori B. The rise of MXenes. ACS Nano 2019;13:8491–4.

[5] Naguib M, Mochalin VN, Barsoum MW, Gogotsi Y. 25th anniversary article: MXenes: a new family of two-dimensional materials. Adv Mater 2014;26:992–1005.

[6] Ding L, Wei Y, Li L, Zhang T, Wang H, Xue J, et al. MXene molecular sieving membranes for highly efficient gas separation. Nat Commun 2018;9:155.

[7] Driscoll N, Maleski K, Richardson AG, Murphy B, Anasori B, Lucas TH, et al. Fabrication of Ti3C2 MXene microelectrode arrays for in vivo neural recording. JoVE 2020:e60741.

[8] Xie X, Chen C, Zhang N, Tang Z-R, Jiang J, Xu Y-J. Microstructure and surface control of MXene films for water purification. Nature Sustainability 2019;2:856–62.

[9] Fan Y, Wei L, Meng X, Zhang W, Yang N, Jin Y, et al. An unprecedented high-temperature-tolerance 2D laminar MXene membrane for ultrafast hydrogen sieving. J Membr Sci 2019;569:117–23.

[10] Ren CE, Hatzell KB, Alhabeb M, Ling Z, Mahmoud KA, Gogotsi Y. Charge-and size-selective ion sieving through Ti3C2T x MXene membranes. J Phys Chem Lett 2015;6:4026–31.

[11] Barsoum MW. The MN+1AXN phases: a new class of solids: thermodynamically stable nanolaminates. Prog Solid State Chem 2000;28:201–81.

[12] Verger L, Xu C, Natu V, Cheng H-M, Ren W, Barsoum MW. Overview of the synthesis of MXenes and other ultrathin 2D transition metal carbides and nitrides. Curr Opin Solid State Mater Sci 2019;23:149–63.

[13] Naguib M, Mochalin Vadym N, Barsoum Michel W, Gogotsi Y. 25th anniversary article: MXenes: a new family of two-dimensional materials. Adv Mater 2013;26:992–1005.

[14] Ghidiu M, Lukatskaya MR, Zhao M-Q, Gogotsi Y, Barsoum MW. Conductive two-dimensional titanium carbide 'clay' with high volumetric capacitance. Nature 2014;516:78.

[15] Anasori B, Lukatskaya MR, Gogotsi Y. 2D metal carbides and nitrides (MXenes) for energy storage. Nature Reviews Materials 2017;2:16098.

[16] Wang J, Chen P, Shi B, Guo W, Jaroniec M, Qiao SZ. A regularly channeled lamellar membrane for unparalleled water and organics permeation. Angew Chem Int Ed 2018;57:6814–8.

[17] Sarycheva A, Polemi A, Liu Y, Dandekar K, Anasori B, Gogotsi Y. 2D titanium carbide (MXene) for wireless communication. Science advances 2018;4:eaau0920.

[18] Fang Y, Yang X, Chen T, Xu G, Liu M, Liu J, et al. Two-dimensional titanium carbide (MXene)-based solid-state electrochemiluminescent sensor for label-free single-nucleotide mismatch discrimination in human urine. Sensor Actuator B Chem 2018;263:400–7.

[19] Han M, Yin X, Wu H, Hou Z, Song C, Li X, et al. Ti3C2 MXenes with modified surface for high-performance electromagnetic absorption and shielding in the X-Band. ACS Appl Mater Interfaces 2016;8:21011–9.

[20] Kong F, He X, Liu Q, Qi X, Zheng Y, Wang R, et al. Improving the electrochemical properties of MXene Ti3C2 multilayer for Li-ion batteries by vacuum calcination. Electrochim Acta 2018;265:140–50.

[21] Zhou J, Zha X, Chen Fan Y, Ye Q, Eklund P, Du S, et al. A two-dimensional zirconium carbide by selective etching of Al3C3 from nanolaminated Zr3Al3C5. Angew Chem 2016;128:5092–7.

[22] Halim J, Kota S, Lukatskaya Maria R, Naguib M, Zhao MQ, Moon Eun J, et al. Synthesis and characterization of 2D molybdenum carbide (MXene). Adv Funct Mater 2016;26:3118–27.

[23] Yu X, Cai X, Cui H, Lee S-W, Yu X-F, Liu B. Fluorine-free preparation of titanium carbide MXene quantum dots with high near-infrared photothermal performances for cancer therapy. Nanoscale 2017;9:17859–64.

[24] Hu T, Hu M, Li Z, Zhang H, Zhang C, Wang J, et al. Interlayer coupling in two-dimensional titanium carbide MXenes. Phys Chem Chem Phys 2016;18:20256–60.

[25] Huang K, Li Z, Lin J, Han G, Huang P. Two-dimensional transition metal carbides and nitrides (MXenes) for biomedical applications. Chem Soc Rev 2018;47:5109–24.

[26] Naguib M, Unocic RR, Armstrong BL, Nanda J. Large-scale delamination of multi-layers transition metal carbides and carbonitrides "MXenes". Dalton Trans 2015;44:9353–8.

[27] Xu C, Wang L, Liu Z, Chen L, Guo J, Kang N, et al. Large-area high-quality 2D ultrathin Mo2C superconducting crystals. Nat Mater 2015;14:1135.

[28] Hu T, Li Z, Hu M, Wang J, Hu Q, Li Q, et al. Chemical origin of termination-functionalized MXenes: Ti3C2T2 as a case study. J Phys Chem C 2017;121:19254–61.

[29] Shen J, Liu G, Huang K, Chu Z, Jin W, Xu N. Subnanometer two-dimensional graphene oxide channels for ultrafast gas sieving. ACS Nano 2016;10:3398–409.

[30] Riazi H, Anayee M, Hantanasirisakul K, Shamsabadi AA, Anasori B, Gogotsi Y, et al. Surface modification of a MXene by an aminosilane coupling agent. Advanced Materials Interfaces 2020;20:1902008.

[31] Dikin DA, Stankovich S, Zimney EJ, Piner RD, Dommett GH, Evmenenko G, et al. Preparation and characterization of graphene oxide paper. Nature 2007;448:457–60.

[32] Jie S, Guozhen L, Yufan J, Quan L, Long C, Kecheng G, et al. 2D MXene nanofilms with tunable gas transport channels. Adv Funct Mater 2018;28:1801511.

[33] Karahan HE, Goh K, Zhang C, Yang E, Yıldırım C, Chuah CY, et al. MXene materials for designing advanced separation membranes. Adv Mater 2020;32:1906697.

[34] Shuck CE, Sarycheva A, Anayee M, Levitt A, Zhu Y, Uzun S, et al. Scalable synthesis of Ti3C2Tx MXene. Adv Eng Mater 2020;22:1901241.

[35] Leung DYC, Caramanna G, Maroto-Valer MM. An overview of current status of carbon dioxide capture and storage technologies. Renew Sustain Energy Rev 2014;39:426–43.

[36] Sholl DS, Lively RP. Seven chemical separations to change the world. Nature 2016;532:435–7.

[37] Li J, Li X, Van der Bruggen B. An MXene-based membrane for molecular separation. Environ Sci: Nano 2020;7:1289–304.

[38] Gin DL, Noble RD. Designing the next generation of chemical separation membranes. Science 2011;332:674–6.

[39] Park HB, Kamcev J, Robeson LM, Elimelech M, Freeman BD. Maximizing the right stuff: the trade-off between membrane permeability and selectivity. Science 2017;356:eaab0530.

[40] Gao J, Feng Y, Guo W, Jiang L. Nanofluidics in two-dimensional layered materials: inspirations from nature. Chem Soc Rev 2017;46:5400–24.

[41] Peng Y, Li Y, Ban Y, Jin H, Jiao W, Liu X, et al. Metal-organic framework nanosheets as building blocks for molecular sieving membranes. Science 2014;346:1356–9.

[42] Younas M, Rezakazemi M, Daud M, Wazir MB, Ahmad S, Ullah N, et al. Recent progress and remaining challenges in post-combustion CO2 capture using Metal-Organic Frameworks (MOFs). Prog Energy Combust Sci 2020;80:100849.

[43] Ahmadipouya S, Heidarian Haris M, Ahmadijokani F, Jarahiyan A, Molavi H, Matloubi Moghaddam F, et al. Magnetic Fe3O4@UiO-66 nanocomposite for rapid adsorption of organic dyes from aqueous solution. J Mol Liq 2021;322:114910.

[44] Ahmadijokani F, Tajahmadi S, Bahi A, Molavi H, Rezakazemi M, Ko F, et al. Ethylenediamine-functionalized Zr-based MOF for efficient removal of heavy metal ions from water. Chemosphere 2021;264:128466.

[45] Ahmadijokani F, Mohammadkhani R, Ahmadipouya S, Shokrgozar A, Rezakazemi M, Molavi H, et al. Superior chemical stability of UiO-66 metal-organic frameworks (MOFs) for selective dye adsorption. Chem Eng J 2020;399:125346.

[46] Mirqasemi MS, Homayoonfal M, Rezakazemi M. Zeolitic imidazolate framework membranes for gas and water purification. Environ Chem Lett 2020;18:1–52.

[47] Varoon K, Zhang X, Elyassi B, Brewer DD, Gettel M, Kumar S, et al. Dispersible exfoliated zeolite nanosheets and their application as a selective membrane. Science 2011;334:72–5.

[48] Kim HW, Yoon HW, Yoon S-M, Yoo BM, Ahn BK, Cho YH, et al. Selective gas transport through few-layered graphene and graphene oxide membranes. Science 2013;342:91–5.

[49] Celebi K, Buchheim J, Wyss RM, Droudian A, Gasser P, Shorubalko I, et al. Ultimate permeation across atomically thin porous graphene. Science 2014;344:289–92.

[50] Rollings RC, Kuan AT, Golovchenko JA. Ion selectivity of graphene nanopores. Nat Commun 2016;7:11408.

[51] Ding L, Wei Y, Wang Y, Chen H, Caro J, Wang H. A two-dimensional lamellar membrane: MXene nanosheet stacks. Angew Chem Int Ed 2017;56:1825–9.

[52] Kim S, Wang H, Lee YM. 2D nanosheets and their composite membranes for water, gas, and ion separation. Angew Chem 2019;131:17674–89.

[53] Zhang CJ, Pinilla S, McEvoy N, Cullen CP, Anasori B, Long E, et al. Oxidation stability of colloidal two-dimensional titanium carbides (MXenes). Chem Mater 2017;29:4848–56.

[54] Zhang Z, Yang S, Zhang P, Zhang J, Chen G, Feng X. Mechanically strong MXene/Kevlar nanofiber composite membranes as high-performance nanofluidic osmotic power generators. Nat Commun 2019;10:1–9.

[55] Gund GS, Park JH, Harpalsinh R, Kota M, Shin JH, Kim T-i, et al. MXene/polymer hybrid materials for flexible AC-filtering electrochemical capacitors. Joule 2019;3:164–76.

[56] Chen C, Boota M, Xie X, Zhao M, Anasori B, Ren CE, et al. Charge transfer induced polymerization of EDOT confined between 2D titanium carbide layers. J Mater Chem 2017;5:5260–5.

[57] Chen J, Chen K, Tong D, Huang Y, Zhang J, Xue J, et al. CO 2 and temperature dual responsive "Smart" MXene phases. Chem Commun 2015;51:314–7.

[58] Zhang Z, Yang S, Zhang P, Zhang J, Chen G, Feng X. Mechanically strong MXene/Kevlar nanofiber composite membranes as high-performance nanofluidic osmotic power generators. Nat Commun 2019;10:2920.

[59] Liu G, Shen J, Ji Y, Liu Q, Liu G, Yang J, et al. Two-dimensional Ti 2 CT x MXene membranes with integrated and ordered nanochannels for efficient solvent dehydration. J Mater Chem 2019;7:12095–104.

[60] Xing Y, Akonkwa G, Liu Z, Ye H, Han K. Crumpled two-dimensional Ti3C2T x MXene lamellar membranes for solvent permeation and separation. ACS Applied Nano Materials 2020;3:1526–34.

[61] Sun Y, Li S, Zhuang Y, Liu G, Xing W, Jing W. Adjustable interlayer spacing of ultrathin MXene-derived membranes for ion rejection. J Membr Sci 2019;591:117350.

[62] Wei S, Xie Y, Xing Y, Wang L, Ye H, Xiong X, et al. Two-dimensional graphene Oxide/MXene composite lamellar membranes for efficient solvent permeation and molecular separation. J Membr Sci 2019;582:414–22.

[63] Arabi Shamsabadi A, Rezakazemi M, Seidi F, Riazi H, Aminabhavi T, Soroush M. Next generation polymers of intrinsic microporosity with tunable moieties for ultrahigh permeation and precise molecular CO2 separation. Prog Energy Combust Sci 2021;84:100903.

[64] Xu WL, Fang C, Zhou F, Song Z, Liu Q, Qiao R, et al. Self-assembly: a facile way of forming ultrathin, high-performance graphene oxide membranes for water purification. Nano Lett 2017;17:2928–33.

[65] Li L, Zhang T, Duan Y, Wei Y, Dong C, Ding L, et al. Selective gas diffusion in two-dimensional MXene lamellar membranes: insights from molecular dynamics simulations. J Mater Chem 2018;6:11734–42.
[66] Shen J, Liu G, Ji Y, Liu Q, Cheng L, Guan K, et al. 2D MXene nanofilms with tunable gas transport channels. Adv Funct Mater 2018;28:1801511.
[67] Arabi Shamsabadi A, Pournaghshband Isfahani A, Khoshhal Salestan S, Rahimpour A, Ghalei B, Sivaniah E, et al. Pushing rubbery polymer membranes to be economic for CO2 separation: embedment with Ti3C2Tx MXene nanosheets. ACS Appl Mater Interfaces 2020;12:3984–92.
[68] Wang S, Wu Y, Zhang N, He G, Xin Q, Wu X, et al. A highly permeable graphene oxide membrane with fast and selective transport nanochannels for efficient carbon capture. Energy Environ Sci 2016;9:3107–12.
[69] Wang B, Wu T, Yu M, Li S, Zhou R, Xing W. Highly ordered nanochannels in a nanosheet-directed thin zeolite nanofilm for precise and fast CO2 separation. Small 2020;16:2002836.
[70] de Vos RM, Verweij H. High-selectivity, high-flux silica membranes for gas separation. Science 1998;279:1710.
[71] Elyassi B, Sahimi M, Tsotsis TT. Silicon carbide membranes for gas separation applications. J Membr Sci 2007;288:290–7.
[72] Wang H, Lin YS. Synthesis and modification of ZSM-5/silicalite bilayer membrane with improved hydrogen separation performance. J Membr Sci 2012;396:128–37.
[73] Shekhawat D, Luebke DR, Pennline HW. A review of carbon dioxide selective membranes: a topical report. United States; 2003.
[74] Yang T, Xiao Y, Chung T-S. Poly-/metal-benzimidazole nano-composite membranes for hydrogen purification. Energy Environ Sci 2011;4:4171–80.
[75] Zhou S, Zou X, Sun F, Ren H, Liu J, Zhang F, et al. Development of hydrogen-selective CAU-1 MOF membranes for hydrogen purification by 'dual-metal-source' approach. Int J Hydrogen Energy 2013;38:5338–47.
[76] Zhang X, Liu Y, Li S, Kong L, Liu H, Li Y, et al. New membrane architecture with high performance: ZIF-8 membrane supported on vertically aligned ZnO nanorods for gas permeation and separation. Chem Mater 2014;26:1975–81.
[77] Li Y, Liang F, Bux H, Yang W, Caro J. Zeolitic imidazolate framework ZIF-7 based molecular sieve membrane for hydrogen separation. J Membr Sci 2010;354:48–54.
[78] Guo H, Zhu G, Hewitt IJ, Qiu S. "Twin copper source" growth of Metal−Organic framework membrane: Cu3(BTC)2 with high permeability and selectivity for recycling H2. J Am Chem Soc 2009;131:1646–7.
[79] Aguado S, Nicolas C-H, Moizan-Baslé V, Nieto C, Amrouche H, Bats N, et al. Facile synthesis of an ultramicroporous MOF tubular membrane with selectivity towards CO2. New J Chem 2011;35:41–4.
[80] Fu J, Das S, Xing G, Ben T, Valtchev V, Qiu S. Fabrication of COF-MOF composite membranes and their highly selective separation of H2/CO2. J Am Chem Soc 2016;138:7673–80.
[81] Li H, Song Z, Zhang X, Huang Y, Li S, Mao Y, et al. Ultrathin, molecular-sieving graphene oxide membranes for selective hydrogen separation. Science 2013;342:95.
[82] Kim HW, Yoon HW, Yoon S-M, Yoo BM, Ahn BK, Cho YH, et al. Selective gas transport through few-layered graphene and graphene oxide membranes. Science 2013;342:91.
[83] Huang A, Liu Q, Wang N, Zhu Y, Caro J. Bicontinuous zeolitic imidazolate framework ZIF-8@GO membrane with enhanced hydrogen selectivity. J Am Chem Soc 2014;136:14686–9.
[84] Achari ASS, Eswaramoorthy M. High performance MoS2 membranes: effects of thermally driven phase transition on CO2 separation efficiency. Energy Environ Sci 2016;9:1224–8.
[85] Wang D, Wang Z, Wang L, Hu L, Jin J. Ultrathin membranes of single-layered MoS2 nanosheets for high-permeance hydrogen separation. Nanoscale 2015;7:17649–52.
[86] Peng Y, Li Y, Ban Y, Jin H, Jiao W, Liu X, et al. Metal-organic framework nanosheets as building blocks for molecular sieving membranes. Science 2014;346:1356.
[87] Wang X, Chi C, Zhang K, Qian Y, Gupta KM, Kang Z, et al. Reversed thermo-switchable molecular sieving membranes composed of two-dimensional metal-organic nanosheets for gas separation. Nat Commun 2017;8:14460.
[88] Wu Y, Ding L, Lu Z, Deng J, Wei Y. Two-dimensional MXene membrane for ethanol dehydration. J Membr Sci 2019;590:117300.
[89] Ding M, Xu H, Chen W, Yang G, Kong Q, Ng D, et al. 2D laminar maleic acid-crosslinked MXene membrane with tunable nanochannels for efficient and stable pervaporation desalination. J Membr Sci 2020;600:117871.
[90] Guan K, Liang F, Zhu H, Zhao J, Jin W. Incorporating graphene oxide into alginate polymer with a cationic intermediate to strengthen membrane dehydration performance. ACS Appl Mater Interfaces 2018;10:13903–13.
[91] Xu YM, Japip S, Chung T-S. Mixed matrix membranes with nano-sized functional UiO-66-type MOFs embedded in 6FDA-HAB/DABA polyimide for dehydration of C1-C3 alcohols via pervaporation. J Membr Sci 2018;549:217–26.
[92] Rezakazemi M, Ebadi Amooghin A, Montazer-Rahmati MM, Ismail AF, Matsuura T. State-of-the-art membrane based CO2 separation using mixed matrix membranes (MMMs): an overview on current status and future directions. Prog Polym Sci 2014;39:817–61.
[93] Rezakazemi M, Sadrzadeh M, Matsuura T. Thermally stable polymers for advanced high-performance gas separation membranes. Prog Energy Combust Sci 2018;66:1–41.
[94] Xu Z, Liu G, Ye H, Jin W, Cui Z. Two-dimensional MXene incorporated chitosan mixed-matrix membranes for efficient solvent dehydration. J Membr Sci 2018;563:625–32.
[95] Al-Hamadani YAJ, Jun B-M, Yoon M, Taheri-Qazvini N, Snyder SA, Jang M, et al. Applications of MXene-based membranes in water purification: a review. Chemosphere 2020;254:126821.
[96] Li R, Zhang L, Shi L, Wang P. MXene Ti3C2: an effective 2D light-to-heat conversion material. ACS Nano 2017;11:3752–9.
[97] Ihsanullah I. Potential of MXenes in water desalination: current status and perspectives. Nano-Micro Lett 2020;12:72.
[98] Ding L, Li L, Liu Y, Wu Y, Lu Z, Deng J, et al. Effective ion sieving with Ti3C2Tx MXene membranes for production of drinking water from seawater. Nature Sustainability 2020;3:296–302.
[99] Joshi R, Carbone P, Wang FC, Kravets VG, Su Y, Grigorieva IV, et al. Precise and ultrafast molecular sieving through graphene oxide membranes. Science 2014;343:752–4.
[100] Surwade SP, Smirnov SN, Vlassiouk IV, Unocic RR, Veith GM, Dai S, et al. Water desalination using nanoporous single-layer graphene. Nat Nanotechnol 2015;10:459–64.
[101] Chen L, Shi G, Shen J, Peng B, Zhang B, Wang Y, et al. Ion sieving in graphene oxide membranes via cationic control of interlayer spacing. Nature 2017;550:380–3.
[102] Huang H, Song Z, Wei N, Shi L, Mao Y, Ying Y, et al. Ultrafast viscous water flow through nanostrand-channelled graphene oxide membranes. Nat Commun 2013;4:2979.
[103] Abraham J, Vasu KS, Williams CD, Gopinadhan K, Su Y, Cherian CT, et al. Tunable sieving of ions using graphene oxide membranes. Nat Nanotechnol 2017;12:546.
[104] Lin L-C, Grossman JC. Atomistic understandings of reduced graphene oxide as an ultrathin-film nanoporous membrane for separations. Nat Commun 2015;6:8335.
[105] Mahmoud KA, Gogotsi Y, Ren CE. Two-dimensional metal carbide desalination membrane. Google Patents. 2018.
[106] Ghidiu M, Lukatskaya MR, Zhao M-Q, Gogotsi Y, Barsoum MW. Conductive two-dimensional titanium carbide 'clay'with high volumetric capacitance. Nature 2014;516:78.
[107] Berdiyorov GR, Madjet ME, Mahmoud KA. Ionic sieving through Ti3C2 (OH) 2 MXene: first-principles calculations. Appl Phys Lett 2016;108:113110.
[108] Ren CE, Alhabeb M, Byles BW, Zhao M-Q, Anasori B, Pomerantseva E, et al. Voltage gated ions sieving through 2D MXene Ti3C2Tx membranes. ACS Applied Nano Materials 2018;1:3644–52.
[109] Zhao C, Wang Q, Zhang H, Passerini S, Qian X. Two-dimensional titanium carbide/RGO composite for high-performance supercapacitors. ACS Appl Mater Interfaces 2016;8:15661–7.
[110] Firouzjaei MD, Shamsabadi AA, Sharifian Gh M, Rahimpour A, Soroush M. A novel nanocomposite with superior antibacterial activity: a silver-based metal organic framework embellished with graphene oxide. Advanced Materials Interfaces 2018;5:1701365.
[111] Seredych M, Shuck CE, Pinto D, Alhabeb M, Precetti E, Deysher G, et al. High-temperature behavior and surface chemistry of carbide MXenes studied by thermal analysis. Chem Mater 2019;31:3324–32.
[112] Ding L, Li L, Liu Y, Wu Y, Lu Z, Deng J, et al. Effective ion sieving with Ti 3 C 2 T x MXene membranes for production of drinking water from seawater. Nature Sustainability 2020;3:296–302.
[113] Liu G, Shen J, Liu Q, Liu G, Xiong J, Yang J, et al. Ultrathin two-dimensional MXene membrane for pervaporation desalination. J Membr Sci 2018;548:548–58.
[114] Pandey RP, Rasool K, Madhavan VE, Aïssa B, Gogotsi Y, Mahmoud KA. Ultrahigh-flux and fouling-resistant membranes based on layered silver/MXene (Ti 3 C 2 T x) nanosheets. J Mater Chem 2018;6:3522–33.
[115] Ding L, Li L, Liu Y, Wu Y, Lu Z, Deng J, et al. Effective ion sieving with Ti 3 C 2 T x MXene membranes for production of drinking water from seawater. Nature Sustainability 2020:1–7.
[116] Hong S, Ming F, Shi Y, Li R, Kim IS, Tang CY, et al. Two-dimensional Ti3C2Tx MXene membranes as nanofluidic osmotic power generators. ACS Nano 2019;13:8917–25.
[117] Goh K, Karahan HE, Wei L, Bae T-H, Fane AG, Wang R, et al. Carbon nanomaterials for advancing separation membranes: a strategic perspective. Carbon 2016;109:694–710.
[118] Patel P. MXene membranes could be an affordable way to harvest energy from saltwater. 2019.
[119] Ding L, Xiao D, Lu Z, Deng J, Wei Y, Caro J, et al. Oppositely charged Ti3C2Tx MXene membranes with 2D nanofluidic channels for osmotic energy harvesting. Angew Chem Int Ed 2020;59:8720–6.
[120] Cheng H, Zhou Y, Feng Y, Geng W, Liu Q, Guo W, et al. Electrokinetic energy conversion in self-assembled 2D nanofluidic channels with Janus nanobuilding blocks. Adv Mater 2017;29:1700177.
[121] Kim D-K, Duan C, Chen Y-F, Majumdar A. Power generation from concentration gradient by reverse electrodialysis in ion-selective nanochannels. Microfluid Nanofluidics 2010;9:1215–24.
[122] Hwang J, Sekimoto T, Hsu W-L, Kataoka S, Endo A, Daiguji H. Thermal dependence of nanofluidic energy conversion by reverse electrodialysis. Nanoscale 2017;9:12068–76.
[123] Tsai T-C, Liu C-W, Yang R-J. Power generation by reverse electrodialysis in a microfluidic device with a nafion ion-selective membrane. Micromachines 2016;7:205.
[124] Xin W, Zhang Z, Huang X, Hu Y, Zhou T, Zhu C, et al. High-performance silk-based hybrid membranes employed for osmotic energy conversion. Nat Commun 2019;10:3876.

[125] Ji J, Kang Q, Zhou Y, Feng Y, Chen X, Yuan J, et al. Osmotic power generation with positively and negatively charged 2D nanofluidic membrane pairs. Adv Funct Mater 2017;27:1603623.

[126] Xiao K, Giusto P, Wen L, Jiang L, Antonietti M. Nanofluidic ion transport and energy conversion through ultrathin free-standing polymeric carbon nitride membranes. Angew Chem Int Ed 2018;57:10123–6.

[127] Zhu X, Hao J, Bao B, Zhou Y, Zhang H, Pang J, et al. Unique ion rectification in hypersaline environment: a high-performance and sustainable power generator system. Science Advances 2018;4:eaau1665.

[128] Li R, Jiang J, Liu Q, Xie Z, Zhai J. Hybrid nanochannel membrane based on polymer/MOF for high-performance salinity gradient power generation. Nanomater Energy 2018;53:643–9.

[129] Gao J, Guo W, Feng D, Wang H, Zhao D, Jiang L. High-performance ionic diode membrane for salinity gradient power generation. J Am Chem Soc 2014;136:12265–72.

[130] Han R, Ma X, Xie Y, Teng D, Zhang S. Preparation of a new 2D MXene/PES composite membrane with excellent hydrophilicity and high flux. RSC Adv 2017;7:56204–10.

[131] Sun Y, Xu Z, Zhuang Y, Liu G, Jin W, Liu G, et al. Tunable dextran retention of MXene-TiO 2 mesoporous membranes by adjusting the 2D MXene content. 2D Mater 2018;5:045003.

[132] Huang H, Mao Y, Ying Y, Liu Y, Sun L, Peng X. Salt concentration, pH and pressure controlled separation of small molecules through lamellar graphene oxide membranes. Chem Commun 2013;49:5963–5.

[133] Sun L, Huang H, Peng X. Laminar MoS2 membranes for molecule separation. Chem Commun 2013;49:10718–20.

[134] Sun L, Ying Y, Huang H, Song Z, Mao Y, Xu Z, et al. Ultrafast molecule separation through layered WS2 nanosheet membranes. ACS Nano 2014;8:6304–11.

[135] Huang H, Song Z, Wei N, Shi L, Mao Y, Ying Y, et al. Ultrafast viscous water flow through nanostrand-channelled graphene oxide membranes. Nat Commun 2013;4:2979.

[136] Gao SJ, Qin H, Liu P, Jin J. SWCNT-intercalated GO ultrathin films for ultrafast separation of molecules. J Mater Chem 2015;3:6649–54.

[137] Zhang R, Ji S, Wang N, Wang L, Zhang G, Li J-R. Coordination-Driven In Situ self-assembly strategy for the preparation of metal–organic framework hybrid membranes. Angew Chem Int Ed 2014;53:9775–9.

[138] Zhang Y, Su Y, Chen W, Peng J, Dong Y, Jiang Z. A feasible post-treatment of drying and rewetting for preparation of high-flux pluronic F127/polyethersulfone nanofiltration membranes. Ind Eng Chem Res 2011;50:4678–85.

[139] Srivastava HP, Arthanareeswaran G, Anantharaman N, Starov VM. Performance of modified poly(vinylidene fluoride) membrane for textile wastewater ultrafiltration. Desalination 2011;282:87–94.

[140] Liang B, Zhang P, Wang J, Qu J, Wang L, Wang X, et al. Membranes with selective laminar nanochannels of modified reduced graphene oxide for water purification. Carbon 2016;103:94–100.

[141] Kumar A, Vemula PK, Ajayan PM, John G. Silver-nanoparticle-embedded antimicrobial paints based on vegetable oil. Nat Mater 2008;7:236.

[142] Hajipour MJ, Fromm KM, Ashkarran AA, de Aberasturi DJ, de Larramendi IR, Rojo T, et al. Antibacterial properties of nanoparticles. Trends Biotechnol 2012;30:499–511.

[143] Rasool K, Pandey RP, Rasheed PA, Buczek S, Gogotsi Y, Mahmoud KA. Water treatment and environmental remediation applications of two-dimensional metal carbides (MXenes). Mater Today 2019;30:80–102.

[144] Richter AP, Brown JS, Bharti B, Wang A, Gangwal S, Houck K, et al. An environmentally benign antimicrobial nanoparticle based on a silver-infused lignin core. Nat Nanotechnol 2015;10:817.

[145] Tu Y, Lv M, Xiu P, Huynh T, Zhang M, Castelli M, et al. Destructive extraction of phospholipids from Escherichia coli membranes by graphene nanosheets. Nat Nanotechnol 2013;8. :nnano. 2013.125.

[146] Mao D, Hu F, Ji S, Wu W, Ding D, Kong D, et al. Metal–organic-Framework-assisted in vivo bacterial metabolic labeling and precise antibacterial therapy. Adv Mater 2018;30:1706831.

[147] Zirehpour A, Rahimpour A, Arabi Shamsabadi A, Sharifian Gh M, Soroush M. Mitigation of thin-film composite membrane biofouling via immobilizing nano-sized biocidal reservoirs in the membrane active layer. Environ Sci Technol 2017;51:5511–22.

[148] Low JJ, Benin AI, Jakubczak P, Abrahamian JF, Faheem SA, Willis RR. Virtual high throughput screening confirmed experimentally: porous coordination polymer hydration. J Am Chem Soc 2009;131:15834–42.

[149] Dadashi Firouzjaei M, Arabi Shamsabadi A, Aghapour Aktij S, Seyedpour SF, Sharifian Gh M, Rahimpour A, et al. Exploiting synergetic effects of graphene oxide and a silver-based metal-organic framework to enhance antifouling and anti-biofouling properties of thin film nanocomposite membranes. ACS Appl Mater Interfaces 2018;10:42967–78.

[150] Akhavan O, Ghaderi E. Toxicity of graphene and graphene oxide nanowalls against bacteria. ACS Nano 2010;4:5731–6.

[151] Rasool K, Helal M, Ali A, Ren CE, Gogotsi Y, Mahmoud KA. Antibacterial activity of Ti3C2T x MXene. ACS Nano 2016;10:3674–84.

[152] Arabi Shamsabadi A, Sharifian Gh M, Anasori B, Soroush M. Antimicrobial mode-of-action of colloidal Ti3C2T x MXene nanosheets. ACS Sustainable Chem Eng 2018;6:16586–96.

[153] Rasool K, Mahmoud KA, Johnson DJ, Helal M, Berdiyorov GR, Gogotsi Y. Efficient antibacterial membrane based on two-dimensional Ti 3 C 2 T x (MXene) nanosheets. Sci Rep 2017;7:1598.

[154] Pandey RP, Rasool K, Vinod E, Aissa B, Gogotsi Y, Mahmoud KA. Ultrahigh-flux and fouling-resistant membrane based on layered silver/MXene (Ti3C2Tx) nanosheets. J Mater Chem 2018;6:3522–33.

[155] Hantanasirisakul K, Gogotsi Y. Electronic and optical properties of 2D transition metal carbides and nitrides (MXenes). Adv Mater 2018;30:1804779.

[156] Zhang CJ, Pinilla S, McEvoy N, Cullen CP, Anasori B, Long E, et al. Oxidation stability of colloidal two-dimensional titanium carbides (MXenes). Chem Mater 2017;29:4848–56.

[157] Habib T, Zhao X, Shah SA, Chen Y, Sun W, An H, et al. Oxidation stability of Ti3C2Tx MXene nanosheets in solvents and composite films. npj 2D Materials and Applications 2019;3:8.

[158] Han F, Luo S, Xie L, Zhu J, Wei W, Chen X, et al. Boosting the yield of MXene 2D sheets via a facile hydrothermal-assisted intercalation. ACS Appl Mater Interfaces 2019;11:8443–52.

[159] Yang S, Zhang P, Wang F, Ricciardulli AG, Lohe MR, Blom PWM, et al. Fluoride-free synthesis of two-dimensional titanium carbide (MXene) using A binary aqueous system. Angew Chem Int Ed 2018;57:15491–5.